Received: 22 July 2020 | Revised: 1 November 2020 | Accepted: 2 November 2020

DOI: 10.1002/cne.25068

RESEARCH ARTICLE

JCN RESEARCH IN SYSTEMS NEUROSCIENCE THE JOURNAL OF COMPARATIVE NEUROLOGY WILEY

Comprehensive map of visual projection neurons for processing ultraviolet information in the *Drosophila* brain

Chu-Yi Tai[1] | **An-Lun Chin**[2] | **Ann-Shyn Chiang**[1,2,3,4,5,6,7]

[1]Institute of Biotechnology, National Tsing Hua University, Hsinchu, Taiwan

[2]Brain Research Center, National Tsing Hua University, Hsinchu, Taiwan

[3]Institute of Systems Neuroscience, National Tsing Hua University, Hsinchu, Taiwan

[4]Graduate Institute of Clinical Medical Science, China Medical University, Taichung, Taiwan

[5]Institute of Molecular and Genomic Medicine, National Health Research Institutes, Miaoli County, Taiwan

[6]Department of Biomedical Science and Environmental Biology, Kaohsiung Medical University, Kaohsiung, Taiwan

[7]Kavli Institute for Brain and Mind, University of California at San Diego, La Jolla, California

Correspondence
Ann-Shyn Chiang, Brain Research Center, National Tsing Hua University, 101, Section 2, Kuang-Fu Road, Hsinchu 30013, Taiwan.
Email: aschiang@life.nthu.edu.tw

Funding information
The Higher Education Sprout Project co-funded by the Ministry of Science and Technology and the Ministry of Education, Taiwan.

Abstract

The brain perceives visual information and controls behavior depending on its underlying neural circuits. How UV information is represented and processed in the brain remains poorly understood. In *Drosophila melanogaster*, UV light is detected by the R7 photoreceptor that projects exclusively into the medulla layer 6 (M_6). Herein, we imaged 28,768 single neurons and identified 238 visual projection neurons linking M_6 to the central brain. Based on morphology and connectivity, these visual projection neurons were systematically classified into 94 cell types belonging to 12 families. Three tracts connected M_6 in each optic lobe to the central brain: One dorsal tract linking to the ipsilateral lateral anterior optic tubercle (L-AOTU) and two medial tracts linking to the ipsilateral ventral medial protocerebrum (VMP) and the contralateral VMP. The M_6 information was primarily represented in the L-AOTU. Each L-AOTU consisted of four columns that each contained three glomeruli. Each L-AOTU glomerulus received inputs from M_6 subdomains and gave outputs to a glomerulus within the ellipsoid body dendritic region, suggesting specific processing of spatial information through the dorsal pathway. Furthermore, the middle columns of the L-AOTUs of both hemispheres were connected via the intertubercle tract, suggesting information integration between the two eyes. In contrast, an ascending neuron linked each VMP to all glomeruli in the bulb and the L-AOTU, bilaterally, suggesting general processing of information through the ventral pathway. Altogether, these diverse morphologies of the visual projection neurons suggested multi-dimensional processing of UV information through parallel and bilateral circuits in the *Drosophila* brain.

KEYWORDS

brain mapping, *Drosophila melanogaster*, spatial navigation, visual pathways

1 | INTRODUCTION

Animal navigation relies on vision to generate a spatial map of the external world in the brain. Insects use UV light as navigation signals to locate the position of the sun (el Jundi et al., 2014; Pfeiffer & Homberg, 2007; Warren et al., 2019). In *Drosophila*, the ellipsoid body

Abbreviations: Neuropil names: EB, **E**llipsoid **B**ody; L-AOTU, **L**ateral **A**nterior **O**ptic **Tu**bercle; BU, **Bu**lb; M_6, **M**edulla layer **6**; VMP, **V**entral **M**edial **P**rotocerebrum; Neuron name (The arrow indicates the direction of information flow. The colons indicate a nondirectional connection): MT, $\mathbf{M}_6$ → L-AO**T**U; MV, $\mathbf{M}_6$ → **V**MP; R7, Retina → M_6; TB, L-AO**T**U → **BU**; TT, L-AO**T**U → L-AO**T**U; VBT, **V**MP → **BU**::L-AO**T**U.

(EB), a ring-shaped structure located at the center of the brain, acts as an internal compass for navigation. The neural activity in EB neurons reflects head orientation during locomotion (Fisher et al., 2019; Kim et al., 2019). However, how UV information is represented in the brain and relayed to the EB remains poorly understood.

The *Drosophila* compound eye is composed of about 750 ommatidia, each containing eight photoreceptors: six outer photoreceptors (R1–R6) and two inner photoreceptors (R7 and R8). The R1–R6 photoreceptors express broadband rhodopsin (Rh1) for motion vision, while the R7 and R8 photoreceptors express different narrowband rhodopsin (Rh3–Rh6) for color vision. Visual information from the eye's photoreceptors is conveyed to the optic lobe, which consists of four neuropils: the lamina, medulla, lobula, and lobula plate. While the lamina receives visual input from the R1–R6 photoreceptors, the medulla, which comprises 10 layers (M1–M10), receives visual input from UV-sensitive R7 photoreceptors and blue-green-sensitive R8 photoreceptors (Behnia & Desplan, 2015; Song & Lee, 2018). Color vision extracts spectral information through synapse interactions between R7 and R8 neurons via reciprocal inhibition (Schnaitmann et al., 2018).

The axons of UV-sensitive R7 neurons terminate exclusively within the layer 6 of the medulla (M_6). Serial-section electron microscopy revealed that amacrine Dm8 neurons with dendritic arbors in the M_6 receive direct synaptic inputs from R7 neurons and connect with transmedulla Tm5c neurons at the lobula. Consistently, functional studies showed that information flows via R7 → Dm8 → Tm5c are necessary for the UV preference behavior in *Drosophila* (Gao et al., 2008; Takemura et al., 2013; Karuppudurai et al., 2014). Conversely, anatomical and functional studies have revealed that other M_6 output neurons known as MT (also, MC61 or MeTu) terminate at the lateral anterior optical tubercle (L-AOTU) are necessary for the phototaxis toward UV light (Otsuna et al., 2014). These results suggested that UV information is diverged from M_6 by different downstream circuits related to control-specific aspects of behavior. However, the M_6 output circuits for processing UV information in the *Drosophila* brain remain to be fully determined.

In this study, we performed a large-scale 3D imaging of single neurons connecting the UV-receiving M_6 to the central brain in *Drosophila*. Our results on the topographical organization of 238 reconstructed M_6 downstream neurons suggested that UV inputs are differentially and hierarchically represented in the brain. Furthermore, the UV information received by the two eyes is integrated and processed in a multilayer manner.

2 | MATERIALS AND METHODS

2.1 | Fly stocks

Fly strains (*Drosophila melanogaster*) were reared on a cornmeal-yeast-agar medium at 25°C with 70% relative humidity under a 12 h/12 h light/dark cycle. Wild type Canton-S flies were used for the generation of the representative model of anterior optic tubercle. The GR-Gal4 and GR-LexA lines were ordered from the Bloomington *Drosophila* Stock Center and the VT-Gal4 lines from the Vienna *Drosophila* Resource Center.

2.2 | Immunohistochemistry

Brain samples were dissected within cold isotonic phosphate-buffered saline (PBS) and fixed immediately in 4% paraformaldehyde in PBS on ice with microwave irradiation (700 W, 90 s, three times). The samples were fixed again in 4% paraformaldehyde in PBS with 0.25% Triton X-100 for another session of microwave irradiation (700 W, 90 s, three times). Moreover, the fixed samples were degassed by vacuum in PBS containing 2% Triton X-100 and 10% normal goat serum (NGS) for 1 h to expel air from the tracheal system and then blocked; then the brain samples were penetrated in the PBS containing 2% Triton X-100 and 10% NGS at 4°C overnight. For immunohistochemistry, brain samples were incubated in PBS containing 0.25% Triton X-100 and 1% NGS with mouse anti-discs large (DLG) antibodies (1:50, antibody 4F3; Developmental Studies Hybridoma Bank [DSHB], University of Iowa, IW) for 2 days at 4°C; biotinylated goat anti-mouse IgG antibodies (1:250, Molecular Probes, Eugene, OR) overnight at room temperature; and Alexa Fluor 635 streptavidin (Molecular Probes, Eugene, OR) overnight at room temperature. Brain samples were extensively washed in PBS containing 1% Triton X-100 and 3% sodium chloride at room temperature for 20 min three times between each step. Finally, the immunolabeled brains were cleared and mounted in the *FocusClear*™ (CelExplorer, Taiwan) for confocal imaging.

2.3 | Confocal imaging and analysis

The morphology of single neurons and expression patterns of driver lines were imaged under a C-Apochromat 40x/N.A 1.2 water immersion objective lens (scanning speed, 7; line average, 4 times; zoom, 0.7; optical slices, 1 μm; resolution, 1024 × 1024 pixels) on a Zeiss LSM710 confocal microscope. The high-resolution L-AOTU and BU models were imaged under a Plan-Apochromat 63x/N.A 1.4 oil immersion objective lens (scanning speed, 6; line average, 8 times; zoom, 0.7; optical slices, 0.5 μm; resolution, 1024 × 1024 pixels). All individual single-neuron images were labeled with the mosaic analysis with a repressible cell marker (MARCM) system (Lee & Luo, 1999) and segmented neurons were warped into the *FlyCircuit* standard brain (*FlyCircuit* database, version 1.2; http://www.flycircuit.tw; Chiang et al., 2011; Shih et al., 2015) with Avizo 9.4.0 (Thermo Fisher Scientific, Waltham, MA), as previously described (Chiang et al., 2011; Shih et al., 2015).

3 | RESULTS

3.1 | Neural tracts that convey M_6 visual information to the central brain

UV-sensing R7 neurons send axonal terminals to M_6. Through the analysis of spatial connectivity between the neuropils of 28,608 single neurons collected in the *FlyCircuit* database, we constructed a comprehensive map of the downstream circuitry of R7 neurons (Figure 1a). The downstream neurons of the M_{R6} were classified into

six families, based on their neuropil connectivity differences (Figure 1b–g). Three neuronal families diverged from the M_6: one family terminated in the ipsilateral L-AOTU via the dorsal tract (named the MT tract, Figure 1b); another family terminated in the ipsilateral VMP via the short medial tract (named the short MV tract, Figure 1c); finally, another family terminated in the contralateral VMP via the long medial tract (named the long MV tract, Figure 1d). Two other neuronal families diverged from the L-AOTU: one terminated in the ipsilateral BU (named the TB tract, Figure 1e) while the other in the contralateral L-AOTU (named the TT tract, Figure 1f). The remaining neuronal family branched from the VMP and bilaterally terminated to the BU and the L-AOTU of both brain hemispheres (named the VBT tract, Figure 1g). Thus, UV information at M_{R6} was relayed to three pairs of neuropils (i.e., L-$AOTU_{RL}$, VMP_{RL}, and BU_{RL}) by six neuronal families. Meanwhile, M_{L6} downstream neurons exhibited mirror circuitry of M_{R6} downstream neurons. Altogether, these results suggested that each of these six neuropils receives UV information from both eyes.

Upon examining the expression patterns of more than 5000 Gal4 and LexA drivers, we identified 22 with a specific expression in MT, TB, or TT neurons (Figure 2 and Table 1). No driver showed specific expression in short MV, long MV, or VBT neurons. To test neuronal connectivity between R7 neurons, MT, TB, and TT neurons, we used the two-color labeling with selected Gal4 drivers expressed in red fluorescent proteins (mKO) and LexA drivers expressed in green fluorescent proteins (GFP). Two-color labeling demonstrated the physical connections that M_6 input R7 neurons overlapped with M_6 output MT neurons in the M_6 (Figure 3a1), L-AOTU input MT neurons overlapped with L-AOTU output TB neurons in the L-AOTU (Figure 3b1), and L-AOTU commissural TT neurons overlapped with L-AOTU output TB neurons in the two L-AOTUs (Figure 3c1, d1). To further confirm synaptic connectivity between pre- and post-synaptic neurons, we used the method of green fluorescent protein reconstitution across synaptic partners (GRASP) with selected Gal4 and LexA drivers respectively expressed two split-GFP fragments—$spGFP_{1\text{-}10}$ and $spGFP_{11}$ (Feinberg et al., 2008). GRASP signal was observed in the synaptic connections between M_6 input R7 neurons and M_6 output MT neurons (Figure 3a2), L-AOTU input MT neurons and L-AOTU output TB neurons (Figure 3b2), and L-AOTU commissural TT neurons and L-AOTU output TB neurons (Figure 3c2,d2). Consequently, these findings suggested that UV information is conveyed from the medulla of the optic lobe to the EB of the central brain via two UV

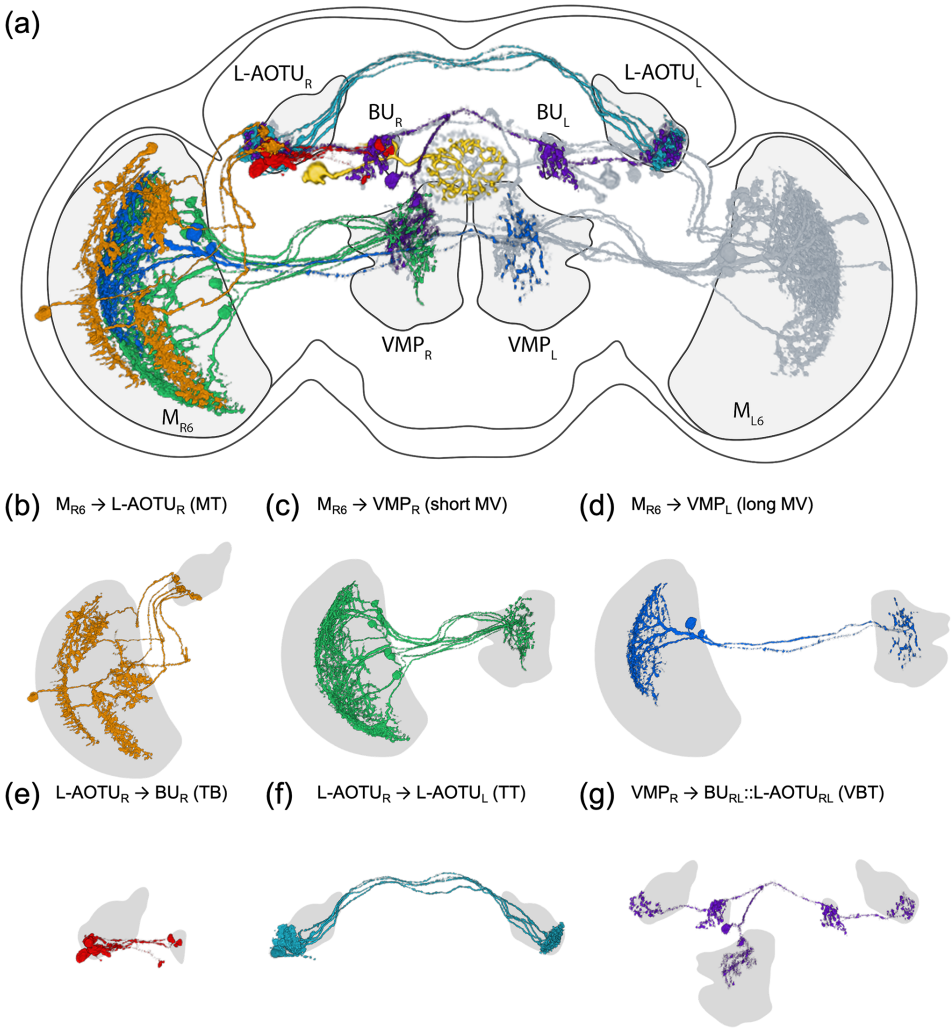

FIGURE 1 Neural tracts that convey medulla layer 6 (M_6) visual information to the central brain. (a) Map of the medulla layer 6 (M_6) downstream circuitry. (b) M_6 output neurons terminate in the ipsilateral lateral anterior optic tubercle (L-AOTU), named the MT tract ($M_{R6} \rightarrow$ L-$AOTU_R$). (c) M_6 output neurons terminate in the ipsilateral ventral medial protocerebrum (VMP), named the short MV tract ($M_{R6} \rightarrow VMP_R$). (d) M_6 output neurons terminate in the contralateral VMP, named the long MV tract ($M_{R6} \rightarrow VMP_L$). (e) L-AOTU output neurons terminate in the ipsilateral bulb (BU), named the TL tract (L-$AOTU_R \rightarrow BU_R$). (f) L-AOTU output neurons terminate in the contralateral L-AOTU, named the TT tract (L-$AOTU_R \rightarrow$ L-$AOTU_L$). (g) A VMP output neuron terminates bilaterally in both the BU and the L-AOTU, named the VBT tract ($VMP_R \rightarrow BU_{RL}$::L-$AOTU_{RL}$). An ellipsoid body (EB) ring neuron is shown in yellow. For clarity, all downstream neurons of the M_{L6} are shown in gray [Color figure can be viewed at wileyonlinelibrary.com]

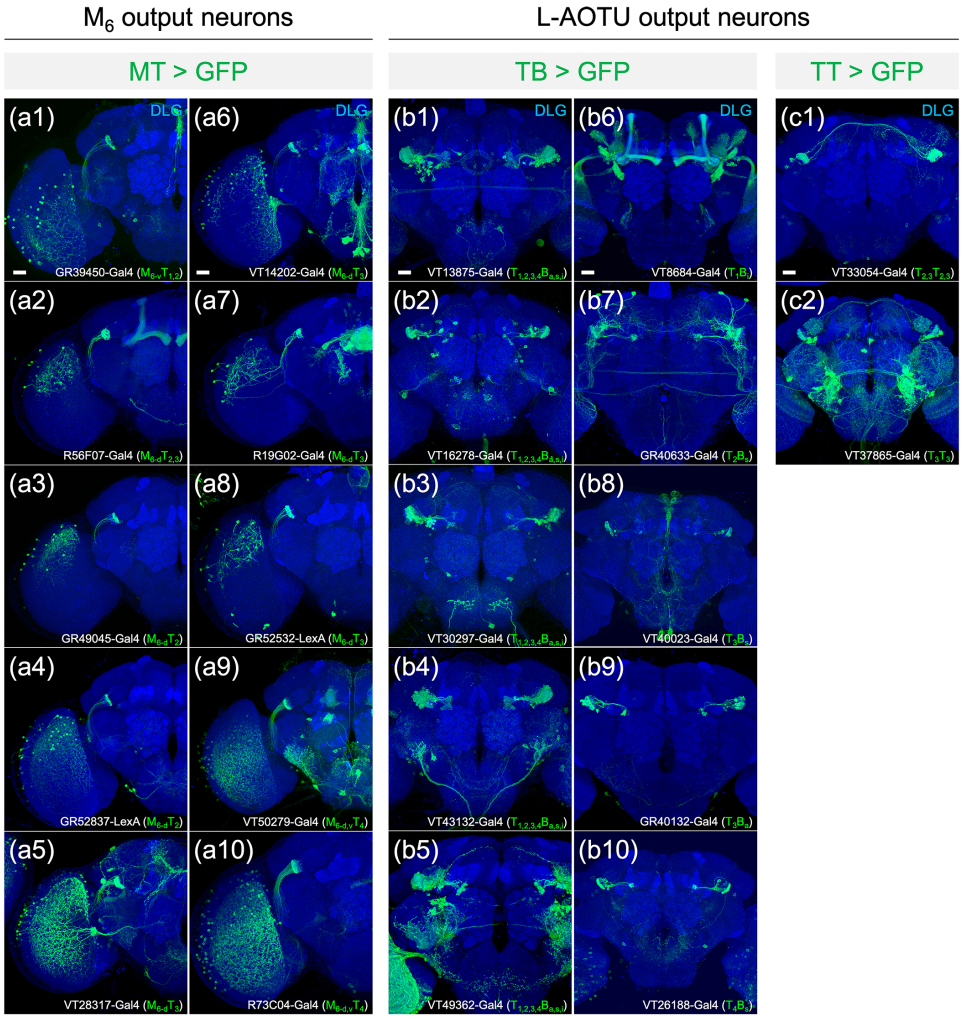

FIGURE 2 Expression patterns of Gal4 and LexA drivers in MT, TB, and TT neurons. (a1–a10) Expression of medulla layer 6 (M_6) output MT neuron drivers. (b1–b10) Expression of lateral anterior optic tubercle (L-AOTU) output TB neuron drivers. (c1–c2) Expression of L-AOTU output TT neurons drivers. GFP expression patterns (green) and names of Gal4 and LexA drivers (bottom). Brain neuropils were immunostained with anti-DLG antibodies (blue). Images are frontal views of confocal projections of several adjacent optical sections unless otherwise specified. Scale bar: 20 μm [Color figure can be viewed at wileyonlinelibrary.com]

pathways, namely, R7 → M_6 → ipsilateral L-AOTU → ipsilateral BU and R7 → M_6 → ipsilateral L-AOTU → contralateral L-AOTU → contralateral BU.

3.2 | The L-AOTU consists of four columns

The L-AOTU is located at the dorsal–frontal surface, between the mushroom body lobes and the lateral horn in each hemisphere (Figure 4a). Previous studies defined three columns in L-AOTU: the medial L-AOTU, the intermediate lateral L-AOTU, and the lateral L-AOTU (Omoto et al., 2017; Timaeus et al., 2020). Here, we performed immunolabeling with anti-DLG antibodies using high-resolution confocal microscopy revealed that the L-AOTU is subdivided into four vertical columns by the aggregation of DLG synaptic proteins (Figure 4b). The obvious boundary allowed us to manually demarcate individual L-AOTU columns (L-AOTU$_1$, L-AOTU$_2$, L-AOTU$_3$, and L-AOTU$_4$) from medial to lateral (Figure 4b1), and to visualize their spatial relationships (Figure 4c). Furthermore, each L-AOTU column expressed Gal4 or LexA drivers in the column-specific input MT tract (Figure 4d1–d4) and the column-specific output TB tract (Figure 4e1–e4). Double labeling with two L-AOTU column-specific drivers showed the four L-AOTU columns in each brain hemisphere in the same fly (Figure 5). Indeed, we found that the R56F07-Gal4 driver, which previously defined as located in the intermediate lateral L-AOTU (Omoto et al., 2017), contains two columns, namely, the L-AOTU$_2$ and the L-AOTU$_3$ (Figure 5a and Table 2). Intriguingly, only the L-AOTU$_2$ and the L-AOTU$_3$ in both hemispheres were linked by the commissural TT tract formed by the L-AOTU$_{R2,R3}$ → L-AOTU$_{L2,L3}$; L-AOTU$_{L2,L3}$ → L-AOTU$_{R2,R3}$; L-AOTU$_{R3}$ → L-AOTU$_{L3}$; and L-AOTU$_{L3}$ → L-AOTU$_{R3}$ neurons (Figure 2c1–c2, and Table 1).

3.3 | Cell typing and nomenclature

We imaged the 160 single neurons that were stochastically labeled by MARCM (Lee & Luo, 1999) using specific Gal4 drivers expressed in M_6 downstream neurons (Figure 2). Together with 78 related neurons in the *FlyCircuit* database, we classified and named a total of 238 R7 downstream neurons (Table 3) into 94 cell types (including predicted types), belonging to 42 subfamilies, 12 families, 6 classes, and 3 superclasses (Figure 6 and Table 3). Neurons of the same cell type were morphologically indistinguishable, connected the same neuropils, and had a similar spatial distribution for both dendritic and axonal

TABLE 1 Characterization of the innervation pattern of 22 drivers expressed in MT, TB, and TT neurons [Color table can be viewed at wileyonlinelibrary.com]

Neuron	Driver	M_6 d	M_6 v	L-AOTU 1	L-AOTU 2	L-AOTU 3	L-AOTU 4	BU a	BU s	BU i	Pattern
MT	GR39450-Gal4		●	●	●						**Fig. 2** a1
	R56F07-Gal4	●			●	●					**Fig. 2** a2
	GR49045-Gal4	●			●						**Fig. 2** a3
	GR52837-LexA	●			●						**Fig. 2** a4
	VT28317-Gal4	●				●					**Fig. 2** a5
	VT14202-Gal4	●				●					**Fig. 2** a6
	R19G02-Gal4	●				●					**Fig. 2** a7
	GR52532-LexA	●				●					**Fig. 2** a8
	VT50279-Gal4	●	●				●				**Fig. 2** a9
	R73C04-Gal4	●	●				●				**Fig. 2** a10
TB	VT13875-Gal4			●	●	●	●	●	●	●	**Fig. 2** b1
	VT16278-Gal4			●	●	●	●	●	●	●	**Fig. 2** b2
	VT30297-Gal4			●	●	●	●	●	●	●	**Fig. 2** b3
	VT43132-Gal4			●	●	●	●	●	●	●	**Fig. 2** b4
	VT49362-Gal4			●	●	●	●	●	●	●	**Fig. 2** b5
	VT8684-Gal4			●						●	**Fig. 2** b6
	GR40633-Gal4				●				●		**Fig. 2** b7
	VT40023-Gal4					●			●		**Fig. 2** b8
	GR40132-Gal4					●		●			**Fig. 2** b9
	VT26188-Gal4						●			●	**Fig. 2** b10
TT	VT33054-Gal4				●	●					**Fig. 2** c1
	VT37865-Gal4					●					**Fig. 2** c2

d: dorsal, v: ventral. a: anterior, s: superior, i: inferior

Abbreviations: a, anterior; d, dorsal; i, inferior; s, superior; v, ventral.

terminals. Neurons with dendrites and axons that innervated the same neuropils belonged to the same family. Within the same family, neurons with axonal terminals distributed in the same neuropil subdivision belonged to the same subfamily. Neurons with dendrites that innervated the same neuropil belonged to the same class. Neurons with mirror morphology between the two hemispheres belonged to the same superclass.

For the systematic analysis of 238 single neurons, each cell type was assigned a simple name based on their dendritic and axonal distributions. For example, $M_{R6\text{-}d} \rightarrow$ L-AOTU$_{R2\text{-}d}$ (named $M_{R6\text{-}d}T_{R2\text{-}d}$, Table 4, and Table 5) represents the MT neuron with dendritic arbors in the dorsal region of the right M_6 and the axon terminals in the dorsal glomerulus of the right L-AOTU$_2$. Upon examining thousands of single-neuron images and driver expressions, we found that these visual projection neurons (VPNs) were highly stereotyped and left–right symmetric in all cases from different individual neurons. This allowed us to predict additional 34 types of M_6 downstream neurons (i.e., $M_{L6\text{-}v} \rightarrow$ L-AOTU$_{L4\text{-}v}$ and $M_{R6\text{-}v} \rightarrow$ L-AOTU$_{R4\text{-}v}$ were predicted from the specific MT$_4$ drivers, while and $M_{L6\text{-}d,v} \rightarrow$ VMP$_{L\text{-}s,i}$ was predicted from the symmetrical neuronal partner, $M_{R6\text{-}d,v} \rightarrow$ VMP$_{R\text{-}s,i}$). Using this systematic nomenclature system, we provided a detailed list of all identified and predicted cell types of the M_6 downstream neurons (See Tables 3 and 4 for VPN nomenclature and synonyms).

3.4 | MT neurons

All MT neurons linked the M_6 to the ipsilateral L-AOTU and shared similar morphology (Figure 7a–b). Each MT neuron had small-field dendritic arbors in the subdomain of the M_6 and axonal terminals in a single glomerulus of the L-AOTU. Based on the differences in the connection between the M_6 subdomains and the L-AOTU glomeruli, we classified the MT neurons into 21 cell types (including predicted cell types) belonging to seven subfamilies in each hemisphere (Figure 6 and Tables 3 and 4 for systematic analysis and a full list of cell types). The dendrites of MT neurons covered the entire M_6 from

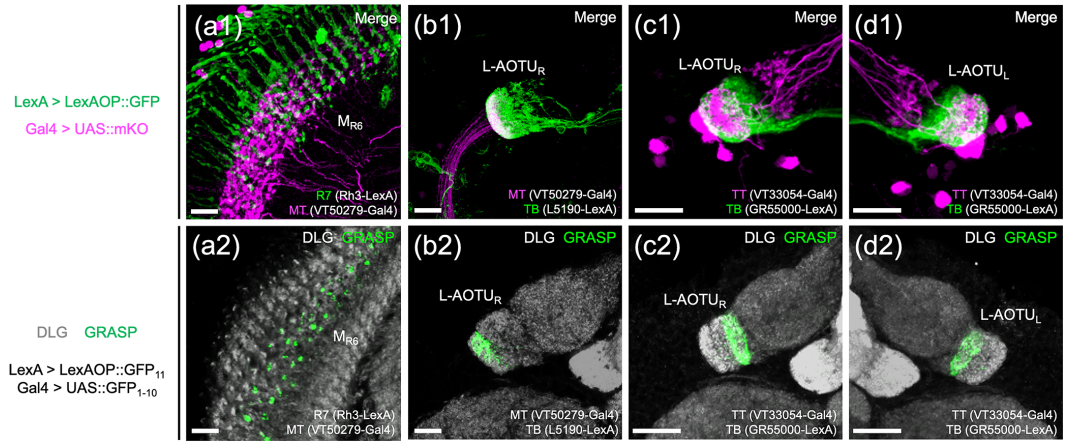

FIGURE 3 Anatomical connection from UV-sensing R7 photoreceptors to the central brain. (a) Connection between R7 and the MT. Overlap of double labeling between R7 (labeled with Rh3-LexA, green) and the MT (labeled with VT50279-Gal4, magenta) in the medulla layer 6 (M_6) (a1). The green fluorescent protein reconstitution across synaptic partners (GRASP) signals between R7 and the MT show in the M_6 (a2). (b) Connection between the MT and the TB. Overlap of double labeling between the MT (labeled with VT50279-Gal4, magenta) and the TB (labeled with L5190-LexA, green) in the lateral anterior optic tubercle (L-AOTU) (b1). The GRASP signals between the MT and the TB show in the L-AOTU (b2). (c–d) Connection between the TB and the TT of the two hemispheres. Overlap of double labeling between the TB (labeled with GR55000-LexA, green) and the TT (labeled with VT33054-Gal4, magenta) in the L-$AOTU_R$ (c1) and the L-$AOTU_L$ (d1). The GRASP signals between the TB and the TT show in the L-$AOTU_R$ (c2) and the L-$AOTU_L$ (d2). Brain neuropils were immunostained with anti-DLG antibodies (gray). Images are frontal views of confocal projections of several adjacent optical sections unless otherwise specified. Scale bar: 20 μm [Color figure can be viewed at wileyonlinelibrary.com]

dorsal to ventral and from anterior to posterior, revealing tilling innervation patterns in the M_6 (Figure 7a–d). The axons of MT neurons further subdivided the L-AOTU into 12 glomeruli, and each L-AOTU column contained three glomeruli from dorsal, medial, to ventral (Figure 7c–d). Altogether, MT neurons exhibited the following wiring principles: (a) L-$AOTU_3$ glomeruli receive visual inputs exclusively from dorsal M_6, but glomeruli in the L-$AOTU_1$, L-$AOTU_2$, and L-$AOTU_4$ receive visual inputs from both the dorsal M_6 and the ventral M_6 (Figure 7e–f); (b) each L-AOTU column receives visual inputs from both the posterior M_6 and the anterior M_6 (as shown by specific MT drivers) (Figure 2a); (c) the dorsal glomerulus of each L-AOTU column receives visual inputs from the posterior M_6, while the ventral glomerulus of each L-AOTU column receives visual inputs from the anterior M_6 (as indicated by a single MT neurons) (Figure 7c–d), consistently with previous reports (Timaeus et al., 2020); and (d) each MT neuron has symmetrical neuronal partners in the contralateral brain hemisphere (i.e., $M_{R6\text{-}d} \rightarrow$ L-$AOTU_{R2\text{-}m}$ and $M_{L6\text{-}d} \rightarrow$ L-$AOTU_{L2\text{-}m}$) (Figure 11a, yellow line).

3.5 | MV neurons

The morphological analysis of thousands of single neurons allowed us to identify two families of M_6 output neurons: one family linking the M_6 to the ipsilateral VMP (named the ipsilateral MV, Figure 7g), and another family linking the M_6 to the contralateral VMP (named the contralateral MV, Figure 7j). The VMP is located at the most posterior region of the brain, below the protocerebral bridge of each hemisphere. Each MV neuron had small-field dendritic arbors in a subdomain of the M_6 and axon terminals in a subdomain of the VMP. Based on the differences in the connections between the M_6 subdomains and the VMP subdomains, the ipsilateral MV neurons and the contralateral MV neurons had three subfamilies and two subfamilies, respectively, per brain hemisphere, and each subfamily only had one cell type (including predicted cell types) (Figure 6 and Tables 3 and 4). The morphology of three types of ipsilateral MV neurons showed that two types had axon terminals in the medial region of the superior and inferior VMPs (Figure 7g1–g2), while the remaining one had axon terminals exclusively in the medial regions of superior VMP (Figure 7g3). Furthermore, all contralateral MV neurons had axon terminals in the medial region of the superior and inferior VMPs (Figure 7j1–j2). Consequently, each VMP receives the convergent visual inputs from both ipsilateral M_6 and contralateral M_6 (Figure 11a, green and blue line).

3.6 | TB neurons

All TB neurons linked the L-AOTU to the ipsilateral BU (Figure 8a–f). Each TB neuron had dendritic arbors in a single glomerulus of the L-AOTU and axon terminals in a single glomerulus of BU. Immunolabeling of synaptic proteins with anti-DLG antibodies revealed that each BU consisted of approximately 80 microglomeruli (Figure 9), which were divided into three groups: ~5 anterior microglomeruli (BU_a), 50 superior microglomeruli (BU_s) and 25 inferior microglomeruli (BU_i) (Figure 9c). Based on the differences in the connections between the 12 glomeruli of the L-AOTU and the three groups of BU microglomeruli, we classified TB neurons into 18 cell

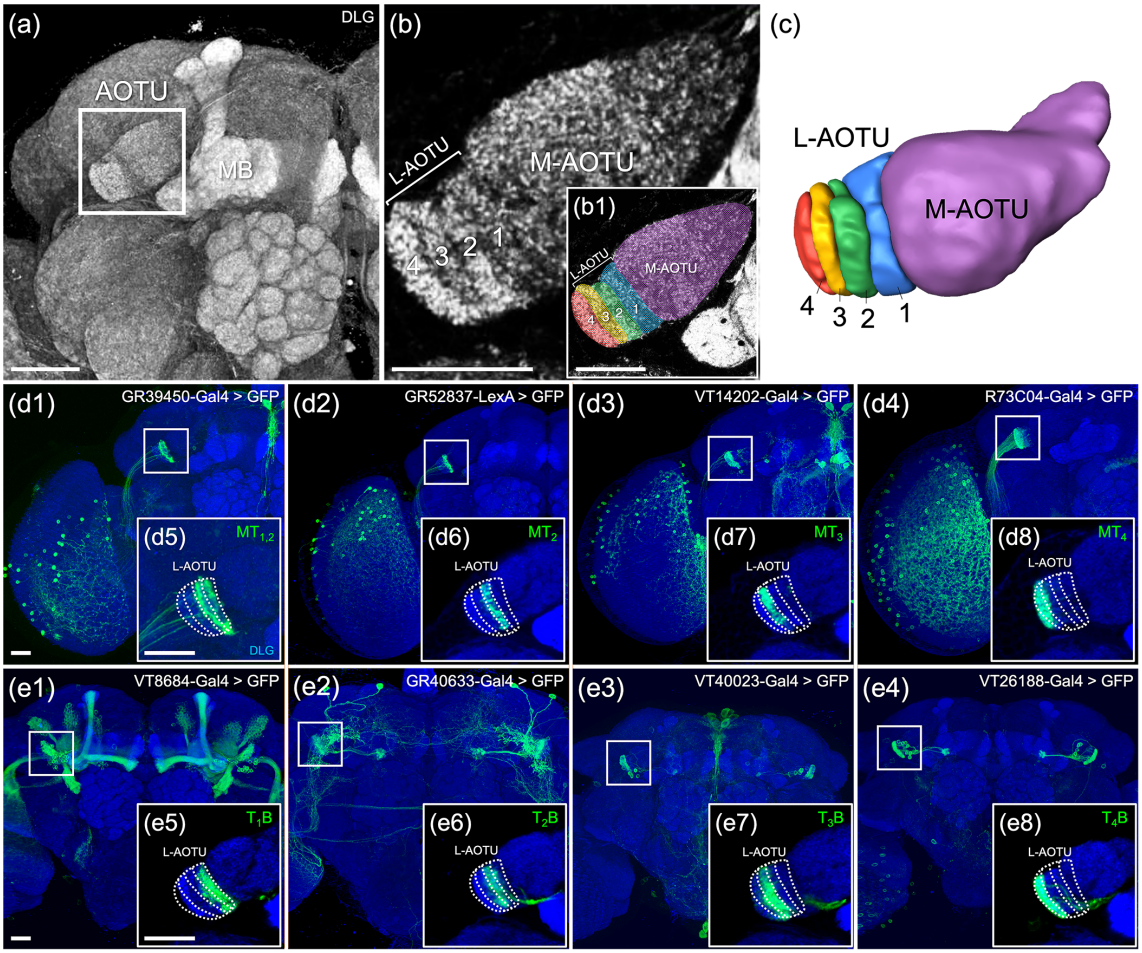

FIGURE 4 The lateral anterior optic tubercle (L-AOTU) consists of four columns. (a) The anterior optic tubercle (AOTU) is located near the frontal surface of the brain at the side of the mushroom (MB). (b) The AOTU consists of the medial AOTU (M-AOTU) and the lateral AOTU (L-AOTU) and locates near the frontal surface of the brain. Imaging of anti-discs large (DLG) stained neuropils (gray) reveals clear structural boundaries, including the vertical strata of the L-AOTU. (b1) Each color reveals a demarcated substructure in the L-AOTU. (c) Volume models of four columns in the L-AOTU. (d1–d4) Expression of column-specific Gal4 and LexA drivers in input MT neurons that were visualized with mCD8::GFP. (d5–d8) High-magnification image in the L-AOTU of column-specific input MT neurons (boxed inset). (e1–e4) Expression of column-specific Gal4 and LexA drivers expressed in output TB neurons that were visualized with mCD8::GFP. (e5–e8) High-magnification image in the L-AOTU of column-specific output TB neurons (boxed inset). Brain structures immunostained with anti-DLG antibodies (gray in a and b; blue in d and e). Images are frontal views of confocal projections of several adjacent optical sections unless otherwise specified. Scale bars: 20 μm [Color figure can be viewed at wileyonlinelibrary.com]

types (including predicted cell types) belonging to six subfamilies in each hemisphere (Figure 6 and Tables 3 and 4 for systematic analysis and a full list of cell types). The dendrites of TB neurons covered the entire L-AOTU glomeruli from the L-AOTU$_1$ to the L-AOTU$_4$, revealing that dendrites of different types of TB neurons overlap in the L-AOTU. Interestingly, we found that TB neurons displayed distinct connections between the L-AOTU columns and the BU groups (Figure 8m). Altogether, single TB neurons (Figure 8a–f) and specific TB drivers (Figure 2b6–b10 and Figure 9d1–d5) demonstrated the following wiring principles: (a) the BU$_a$ receives visual inputs exclusively from the glomeruli in the L-AOTU$_3$ (Figure 8j); (b) the BU$_s$ receive convergent visual inputs from the glomeruli in three consecutive columns (i.e., L-AOTU$_{R2}$ → BU$_{R\text{-}s}$, L-AOTU$_{R3}$ → BU$_{R\text{-}s}$, and L-AOTU$_{R4}$ → BU$_{R\text{-}s}$) (Figure 8h, k, and l); (c) the BU$_i$ receives convergent visual inputs from the glomeruli in two consecutive columns (i.e., L-AOTU$_{R1}$ → BU$_{R\text{-}i}$ and L-AOTU$_{R2}$ → BU$_{R\text{-}i}$) (Figure 8g, i); and (d) each TB neuron has symmetrical neuronal partners in the contralateral brain hemisphere (i.e., L-AOTU$_{R2\text{-}d}$ → BU$_{R\text{-}s}$ and L-AOTU$_{L2\text{-}d}$ → BU$_{L\text{-}s}$) (Figure 11a, red line).

3.7 | TT neurons

All TT neurons connected two L-AOTUs between the two brain hemispheres (Figure 8n). Each TT neuron had dendritic arbors in the multiple glomeruli of two L-AOTU middle columns and axon terminals in the same glomeruli of the contralateral L-AOTU. Based on the differences in the connection between the L-AOTU glomeruli of the two hemispheres, we classified TT neurons into two cell types belonging to one family in each hemisphere (Figure 6 and Tables 3 and 4). One

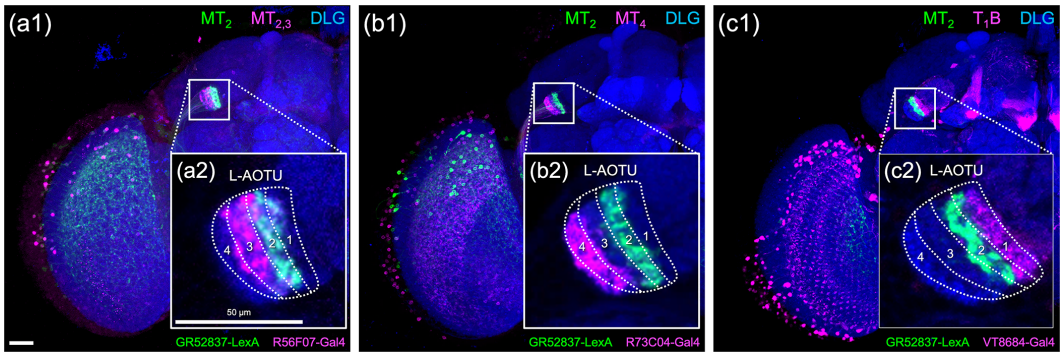

FIGURE 5 Double labeling revealed the lateral anterior optic tubercle (L-AOTU) contains four columns. Double labeling of column-specific MT and TB drivers. (a) The axonal innervation of MT_2 is in L-$AOTU_2$ (labeled with GR52837-LexA, green) and the axonal innervation of $MT_{2,3}$ is in L-$AOTU_{2,3}$ (labeled with R56F07-Gal4, magenta), confirming previous findings that the intermediate lateral L-AOTU is L-$AOTU_2$ and L-$AOTU_3$. (b) The axonal innervation of MT_2 is in L-$AOTU_2$ (labeled with GR52837-LexA, green) and the axonal innervation of MT_4 is in L-$AOTU_4$ (labeled with R73C04-Gal4, magenta), confirming previous findings that the lateral L-AOTU is L-$AOTU_4$. (c) The axonal innervation of MT_2 is in L-$AOTU_2$ (labeled with GR52837-LexA, green) and the dendritic innervation of T_1B is in L-$AOTU_1$ (labeled with VT8684-Gal4, magenta). (a2–c2) High-magnification image of the L-AOTU (boxed inset). Brain structures immunostained with anti-DLG antibodies (blue). Images are frontal views of confocal projections of several adjacent optical sections unless otherwise specified. Scale bars: 20 μm (a1–c1) and 50 μm (a2–c2) [Color figure can be viewed at wileyonlinelibrary.com]

TABLE 2 Comparison of lateral anterior optic tubercle (L-AOTU) subdivisions from the current study and previous studies

Current study (2020)		Omoto et al. (2017)		Timaeus et al. (2020)	
1	VT8684-Gal4	Intermediate (**im**)	R25C04-Gal4	Medial (**m**)	R20B05-LexA
2	GR40683-Gal4	Intermediate lateral (**il**)	R56F07-Gal4	Central (**c**)	Anti-connectin
3	VT40023-Gal4				
4	R73C04-Gal4	Lateral (**l**)	R73C04-Gal4	Lateral (**l**)	R85F05-Gal4

cell type had dendrites innervating six glomeruli in two ipsilateral L-AOTU columns, with the axons terminating in the symmetric glomeruli in two contralateral L-AOTU columns (i.e., L-$AOTU_{R2\text{-}R3}$ → L-$AOTU_{L2\text{-}L3}$ or L-$AOTU_{L2\text{-}L3}$ → L-$AOTU_{R2\text{-}R3}$) (Figure 8n1). The other cell type had dendrites innervating three glomeruli in the ipsilateral L-$AOTU_3$, with the axons terminating in the symmetric glomeruli in the contralateral L-$AOTU_3$ (i.e., L-$AOTU_{R3}$ → L-$AOTU_{L3}$ or L-$AOTU_{L3}$ → L-$AOTU_{R3}$) (Figure 8n2). Altogether, single TT neurons (Figure 8o–p) and specific TT drivers (Figures 2c1–c2) showed the following wiring principle: two L-AOTU middle columns receive and exchange the convergent visual inputs from MT neurons on both sides of the brain (Figure 11a, cyan line).

3.8 | VBT neurons

The identification of the MV neurons allowed us to ask how visual information is conveyed to the EB from the VMP. Through the analysis of thousands of single neurons, we found an ascending neuron, the unique VMP output neuron, linking the unilateral VMP to the bilateral BU and the bilateral L-AOTU (named VBT, Figure 10a). The VBT neurons had one cell type belonging to one subfamily in each hemisphere (Figure 6 and Tables 3 and 4). Each VBT neuron had dendritic arbors in the superior VMP and axon terminals in the three groups of the bilateral BU and further extended to four columns of the bilateral L-AOTU (Figure 10b–c). Consequently, the VBT neuron had a symmetrical neuronal partner showing the mirror wiring diagram in the contralateral brain hemisphere (i.e., $VMP_{R\text{-}s}$ → $BU_{R\text{-}a,s,i,L\text{-}a,s,i}$::L-$AOTU_{R1\text{-}R4,L1\text{-}L4}$ and $VMP_{L\text{-}s}$ → $BU_{L\text{-}a,s,i,R\text{-}a,s,i}$::L-$AOTU_{L1\text{-}L4,R1\text{-}R4}$) (Figure 11a, purple line). These results seemed to indicate that each BU receives the visual inputs from the ipsilateral M_6 and the contralateral M_6 via three parallel pathways: a dorsal tract from the ipsilateral L-AOTU and two medial tracts from the ipsilateral VMP and the contralateral VMP.

4 | DISCUSSION

In this study, we provided a comprehensive map of single VPNs of the M_6 downstream circuitry in the *Drosophila* brain. We identified and classified 238 VPNs into 94 cell types belonging to 12 families, based on their 3D morphology. Classification of these single neurons based on connectivity and specific Gal4 expression allowed us to refine distinct partitions of brain regions involved in UV information processing. The stereotyped circuit organization suggested that environment UV light is hierarchically represented in the brain, which integrates and

TABLE 3 Neurons are identified from *Flycircuit* (orange), selected Gal4 (blue), and predicted type (gray) [Color table can be viewed at wileyonlinelibrary.com]

Superclass	Class	Family	Subfamily	Type	ID
M_6	M_{R6}	M_{R6} → L-AOTU$_R$*	$M_{R6\text{-}d}$ → L-AOTU$_{R1}$	$M_{R6\text{-}d}$ → L-AOTU$_{R1\text{-}d}$	predicted
				$M_{R6\text{-}d}$ → L-AOTU$_{R1\text{-}m}$	predicted
				$M_{R6\text{-}d}$ → L-AOTU$_{R1\text{-}v}$	predicted
			$M_{R6\text{-}d}$ → L-AOTU$_{R2}$	$M_{R6\text{-}d}$ → L-AOTU$_{R2\text{-}d}$	FCT_Cha-F-800020
					VT50279-MARCM-500004
				$M_{R6\text{-}d}$ → L-AOTU$_{R2\text{-}m}$	FCT_Cha-F-500233
					FCT_Cha-F-600239
					FCT_Cha-F-600263
				$M_{R6\text{-}d}$ → L-AOTU$_{R2\text{-}v}$	predicted
			$M_{R6\text{-}d}$ → L-AOTU$_{R3}$	$M_{R6\text{-}d}$ → L-AOTU$_{R3\text{-}d}$	VT50279-MARCM-500002
					VT28317-MARCM-500024
					VT28317-MARCM-500029
					VT28317-MARCM-500034
					VT28317-MARCM-500035
					VT28317-MARCM-600002
					VT28317-MARCM-600014
					VT28317-MARCM-600016
					VT28317-MARCM-600024
					VT28317-MARCM-600027
					VT28317-MARCM-600028
					VT28317-MARCM-600033
					VT28317-MARCM-600038
					VT28317-MARCM-600040
				$M_{R6\text{-}d}$ → L-AOTU$_{R3\text{-}m}$	VT28317-MARCM-500006
					VT28317-MARCM-500011
					VT28317-MARCM-500023
					VT28317-MARCM-500026
					VT28317-MARCM-500027
					VT28317-MARCM-600012
					VT28317-MARCM-600015
					VT28317-MARCM-600032
					VT28317-MARCM-600039
				$M_{R6\text{-}d}$ → L-AOTU$_{R3\text{-}v}$	VT50279-MARCM-500006
			$M_{R6\text{-}d}$ → L-AOTU$_{R4}$	$M_{R6\text{-}d}$ → L-AOTU$_{R4\text{-}d}$	predicted
				$M_{R6\text{-}d}$ → L-AOTU$_{R4\text{-}m}$	predicted
				$M_{R6\text{-}d}$ → L-AOTU$_{R4\text{-}v}$	predicted
			$M_{R6\text{-}v}$ → L-AOTU$_{R1}$	$M_{R6\text{-}v}$ → L-AOTU$_{R1\text{-}d}$	predicted
				$M_{R6\text{-}v}$ → L-AOTU$_{R1\text{-}m}$	predicted
				$M_{R6\text{-}v}$ → L-AOTU$_{R1\text{-}v}$	FCT_Cha-F-400194
			$M_{R6\text{-}v}$ → L-AOTU$_{R2}$	$M_{R6\text{-}v}$ → L-AOTU$_{R2\text{-}d}$	FCT_Gad1-F-200218
				$M_{R6\text{-}v}$ → L-AOTU$_{R2\text{-}m}$	FCT_Cha-F-300281
				$M_{R6\text{-}v}$ → L-AOTU$_{R2\text{-}v}$	FCT_Gad1-F-400023

Note: *The corresponding name previously used in Drosophila.
**The corresponding name previously used in Drosophila.

TABLE 3 Continued

		$M_{R6\text{-}v}$ → L-AOTU$_{R4}$	$M_{R6\text{-}v}$ → L-AOTU$_{R4\text{-}d}$	predicted
			$M_{R6\text{-}v}$ → L-AOTU$_{R4\text{-}m}$	predicted
			$M_{R6\text{-}v}$ → L-AOTU$_{R4\text{-}v}$	predicted
	M_{R6} → VMP$_R$	$M_{R6\text{-}d,v}$ → VMP$_{R\text{-}s,i}$	$M_{R6\text{-}d,v}$ → VMP$_{R\text{-}s,i}$	FCT_VGlut-F-000152
				FCT_VGlut-F-300401
				FCT_VGlut-F-400842
		$M_{R6\text{-}d}$ → VMP$_{R\text{-}s,i}$	$M_{R6\text{-}d}$ → VMP$_{R\text{-}s,i}$	FCT_fru-F-000111
				FCT_fru-F-100051
				FCT_fru-F-100096
				FCT_fru-F-200085
				FCT_fru-F-200153
				FCT_fru-F-300111
				FCT_fru-F-400057
				FCT_fru-F-400341
				FCT_fru-F-600005
				FCT_fru-F-700013
				FCT_fru-F-700059
				FCT_fru-F-800102
				FCT_fru-F-900027
		$M_{R6\text{-}v}$ → VMP$_{R\text{-}s}$	$M_{R6\text{-}v}$ → VMP$_{R\text{-}s}$	FCT_Cha-F-100157
				FCT_Cha-F-100317
				FCT_Cha-F-200296
				FCT_Cha-F-400329
				FCT_Cha-F-700035
	M_{R6} → VMP$_L$	$M_{R6\text{-}d}$ → VMP$_{L\text{-}s,i}$	$M_{R6\text{-}d}$ → VMP$_{L\text{-}s,i}$	FCT_VGlut-F-000513
		$M_{R6\text{-}m}$ → VMP$_{L\text{-}s,i}$	$M_{R6\text{-}m}$ → VMP$_{L\text{-}s,i}$	FCT_Cha-F-200358
M_{L6}	M_{L6} → L-AOTU$_L$*	$M_{L6\text{-}d}$ → L-AOTU$_{L1}$	$M_{L6\text{-}d}$ → L-AOTU$_{L1\text{-}d}$	predicted
			$M_{L6\text{-}d}$ → L-AOTU$_{L1\text{-}m}$	predicted
			$M_{L6\text{-}d}$ → L-AOTU$_{L1\text{-}v}$	FCT_Cha-F-300374
		$M_{L6\text{-}d}$ → L-AOTU$_{L2}$	$M_{L6\text{-}d}$ → L-AOTU$_{L2\text{-}d}$	predicted
			$M_{L6\text{-}d}$ → L-AOTU$_{L2\text{-}m}$	FCT_Cha-F-400261
			$M_{L6\text{-}d}$ → L-AOTU$_{L2\text{-}v}$	predicted
		$M_{L6\text{-}d}$ → L-AOTU$_{L3}$	$M_{L6\text{-}d}$ → L-AOTU$_{L3\text{-}d}$	FCT_Cha-F-300285
				VT50279-MARCM-500001
				VT28317-MARCM-500009
				VT28317-MARCM-500010
				VT28317-MARCM-500012
				VT28317-MARCM-500014
				VT28317-MARCM-500017
				VT28317-MARCM-500031
				VT28317-MARCM-600013
				VT28317-MARCM-600022
				VT28317-MARCM-600023
				VT28317-MARCM-600026
				VT28317-MARCM-600029
				VT28317-MARCM-600031
				VT28317-MARCM-600036
				VT28317-MARCM-600037

TABLE 3 Continued

					VT28317-MARCM-600041
				M_{R6-d} → L-AOTU$_{R3-m}$	VT28317-MARCM-500005
					VT28317-MARCM-500007
					VT28317-MARCM-500019
					VT28317-MARCM-600030
				M_{L6-d} → L-AOTU$_{L3-v}$	FCT_Cha-F-300436
					FCT_Cha-F-700272
					VT28317-MARCM-500020
					VT28317-MARCM-500028
			M_{L6-d} → L-AOTU$_{L4}$	M_{L6-d} → L-AOTU$_{L4-d}$	predicted
				M_{L6-d} → L-AOTU$_{L4-m}$	predicted
				M_{L6-d} → L-AOTU$_{L4-v}$	predicted
			M_{L6-v} → L-AOTU$_{L1}$	M_{L6-v} → L-AOTU$_{L1-d}$	predicted
				M_{L6-v} → L-AOTU$_{L1-m}$	predicted
				M_{L6-v} → L-AOTU$_{L1-v}$	predicted
			M_{L6-v} → L-AOTU$_{L2}$	M_{L6-v} → L-AOTU$_{L2-d}$	predicted
				M_{L6-v} → L-AOTU$_{L2-m}$	predicted
				M_{L6-v} → L-AOTU$_{L2-v}$	predicted
			M_{L6-v} → L-AOTU$_{L4}$	M_{L6-v} → L-AOTU$_{L4-d}$	VT50279-MARCM-500003
					VT50279-MARCM-600001
				M_{L6-v} → L-AOTU$_{L4-m}$	VT50279-MARCM-600002
				M_{L6-v} → L-AOTU$_{L4-v}$	predicted
		M_{L6} → VMP$_{L}$	$M_{L6-d,v}$ → VMP$_{L-s,i}$	$M_{L6-d,v}$ → VMP$_{L-s,i}$	predicted
			M_{L6-d} → VMP$_{L-s,i}$	M_{L6-d} → VMP$_{L-s,i}$	FCT_fru-F-000012
					FCT_fru-F-000230
					FCT_fru-F-200101
					FCT_fru-F-300054
					FCT_fru-F-300092
					FCT_fru-F-300120
					FCT_fru-F-300130
					FCT_fru-F-400249
					FCT_fru-F-400316
					FCT_fru-F-400366
					FCT_fru-F-500578
					FCT_fru-F-700157
					FCT_fru-F-800052
					FCT_fru-F-800083
					FCT_fru-F-900039
					FCT_fru-F-900040
			M_{L6-v} → VMP$_{L-s}$	M_{L6-v} → VMP$_{L-s}$	FCT_VGlut-F-300446
		M_{L6} → VMP$_{R}$	M_{L6-d} → VMP$_{R-s,i}$	M_{L6-d} → VMP$_{R-s,i}$	FCT_VGlut-F-300494
					FCT_fru-F-400331
			M_{L6-m} → VMP$_{R-s,i}$	M_{L6-m} → VMP$_{R-s,i}$	predicted
L-AOTU	L-AOTU$_{R}$	L-AOTU$_{R}$ → BU$_{R}$**	L-AOTU$_{R1}$ → BU$_{R-i}$	L-AOTU$_{R1-d}$ → BU$_{R-i}$	VT13875-F-500000
					VT16278-F-300007
				L-AOTU$_{R1-m}$ → BU$_{R-i}$	VT30297-F-300018
					VT30297-F-300020
				L-AOTU$_{R1-v}$ → BU$_{R-i}$	VT13875-F-200001

TABLE 3 Continued

		VT13875-F-300013
		VT16278-F-300022
		VT16278-F-400009
		VT30297-F-300002
		VT30297-F-300013
		VT43132-F-300005
		VT43132-F-400008
L-AOTU$_{R2}$ → BU$_{R-s}$	L-AOTU$_{R2-d}$ → BU$_{R-s}$	VT13875-F-400011
		VT43132-F-300002
		VT43132-F-300011
		VT43132-F-300012
		VT43132-F-400003
		VT43132-F-400006
	L-AOTU$_{R2-m}$ → BU$_{R-s}$	FCT_Gad1-F-800048
		VT30297-F-400004
		VT43132-F-300004
		VT49362-F-400001
	L-AOTU$_{R2-v}$ → BU$_{R-s}$	VT13875-F-400010
		VT43132-F-400010
		VT43132-F-500000
		VT43132-F-500001
L-AOTU$_{R2}$ → BU$_{R-i}$	L-AOTU$_{R2-d}$ → BU$_{R-i}$	predicted
	L-AOTU$_{R2-m}$ → BU$_{R-i}$	FCT_Cha-F-600054
		VT13875-F-400005
	L-AOTU$_{R2-v}$ → BU$_{R-i}$	VT13875-F-300012
L-AOTU$_{R3}$ → BU$_{R-a}$	L-AOTU$_{R3-d}$ → BU$_{R-a}$	VT49362-F-300002
	L-AOTU$_{R3-m}$ → BU$_{R-a}$	FCT_Gad1-F-300074
		VT13875-F-300000
		VT13875-F-300010
		VT13875-F-500005
		VT49362-F-300003
	L-AOTU$_{R3-v}$ → BU$_{R-a}$	FCT_Cha-F-200155
		VT13875-F-500001
		VT30297-F-300011
L-AOTU$_{R3}$ → BU$_{R-s}$	L-AOTU$_{R3-d}$ → BU$_{R-s}$	VT16278-F-300027
	L-AOTU$_{R3-m}$ → BU$_{R-s}$	FCT_Cha-F-800034
		VT13875-F-300019
		VT13875-F-500003
		VT30297-F-300003
	L-AOTU$_{R3-v}$ → BU$_{R-s}$	FCT_Gad1-F-200129
		VT13875-F-200000
		VT13875-F-300014
		VT16278-F-300002
		VT16278-F-300010
		VT16278-F-300011
		VT30297-F-300000
		VT30297-F-300006
		VT30297-F-300008

TABLE 3 Continued

				VT30297-F-400000
				VT43132-F-300003
				VT43132-F-300006
				VT43132-F-400001
				VT49362-F-300010
		L-AOTU$_{R4}$ → BU$_{R-s}$	L-AOTU$_{R4-d}$ → BU$_{R-s}$	VT13875-F-300018
				VT16278-F-400004
				VT49362-F-300004
			L-AOTU$_{R4-m}$ → BU$_{R-s}$	VT16278-F-300023
				VT16278-F-400005
				VT43132-F-400016
			L-AOTU$_{R4-v}$ → BU$_{R-s}$	FCT_Cha-F-600234
				FCT_Gad1-F-700209
				VT16278-F-300005
				VT16278-F-300013
				VT16278-F-500000
				VT43132-F-400002
	L-AOTU$_{R}$ → L-AOTU$_{L}$	L-AOTU$_{R2-R3}$ → L-AOTU$_{L2-L3}$	L-AOTU$_{R2-R3}$ → L-AOTU$_{L2-L3}$	FCT_fru-F-200039
				FCT_Gad1-F-700269
				FCT_VGlut-F-000541
		L-AOTU$_{R3}$ → L-AOTU$_{L3}$	L-AOTU$_{R3}$ → L-AOTU$_{L3}$	FCT_VGlut-F-000019
				FCT_VGlut-F-400669
L-AOTU$_{L}$	L-AOTU$_{L}$ → BU$_{L}$**	L-AOT$_{L1}$ → BU$_{L-i}$	L-AOTU$_{L1-d}$ → BU$_{L-i}$	FCT_Cha-F-000503
			L-AOTU$_{L1-m}$→ BU$_{L-i}$	VT30297-F-300014
				VT49362-F-300000
			L-AOTU$_{L1-v}$ → BU$_{L-i}$	VT13875-F-300026
				VT16278-F-300000
				VT16278-F-300014
				VT30297-F-300004
				VT30297-F-300005
				VT30297-F-300012
				VT30297-F-300019
				VT43132-F-400015
		L-AOTU$_{L2}$ → BU$_{L-s}$	L-AOTU$_{L2-d}$ → BU$_{L-s}$	FCT_Gad1-F-400100
				VT13875-F-400000
				VT43132-F-300000
				VT43132-F-400011
			L-AOTU$_{L2-m}$ → BU$_{L-s}$	FCT_Cha-F-600079
				FCT_Gad1-F-100297
				VT16278-F-300006
				VT43132-F-400014
				VT49362-F-400000
			L-AOTU$_{L2-v}$ → BU$_{L-s}$	FCT_Gad1-F-000099
				FCT_Gad1-F-000140
				VT16278-F-300004
				VT16278-F-300024
				VT16278-F-300025
				VT30297-F-400003

TABLE 3 Continued

			$L\text{-}AOTU_{L2} \rightarrow BU_{L\text{-}i}$	$L\text{-}AOTU_{L2\text{-}d} \rightarrow BU_{L\text{-}i}$	predicted
				$L\text{-}AOTU_{L2\text{-}m} \rightarrow BU_{L\text{-}i}$	VT13875-F-400006
					VT30297-F-300010
				$L\text{-}AOTU_{L2\text{-}v} \rightarrow BU_{L\text{-}i}$	predicted
			$L\text{-}AOTU_{L3} \rightarrow BU_{L\text{-}a}$	$L\text{-}AOTU_{L3\text{-}d} \rightarrow BU_{L\text{-}a}$	predicted
				$L\text{-}AOTU_{L3\text{-}m} \rightarrow BU_{L\text{-}a}$	VT13875-F-300008
				$L\text{-}AOTU_{L3\text{-}v} \rightarrow BU_{L\text{-}a}$	VT13875-F-300004
			$L\text{-}AOTU_{L3} \rightarrow BU_{L\text{-}s}$	$L\text{-}AOTU_{L3\text{-}d} \rightarrow BU_{L\text{-}s}$	FCT_Cha-F-100098
					VT13875-F-300027
				$L\text{-}AOTU_{L3\text{-}m} \rightarrow BU_{L\text{-}s}$	FCT_Cha-F-400177
					VT13875-F-300021
					VT16278-F-400001
					VT49362-F-300005
				$L\text{-}AOTU_{L3\text{-}v} \rightarrow BU_{L\text{-}s}$	VT13875-F-300020
					VT13875-F-400007
					VT16278-F-300003
					VT16278-F-300008
					VT16278-F-300016
					VT16278-F-300030
					VT30297-F-300015
					VT30297-F-300016
					VT43132-F-300008
					VT43132-F-400000
					VT43132-F-400004
					VT49362-F-300009
					VT49362-F-300011
					VT49362-F-300012
			$L\text{-}AOTU_{L4} \rightarrow BU_{L\text{-}s}$	$L\text{-}AOTU_{L4\text{-}d} \rightarrow BU_{L\text{-}s}$	VT16278-F-400007
				$L\text{-}AOTU_{L4\text{-}m} \rightarrow BU_{L\text{-}s}$	VT16278-F-300001
				$L\text{-}AOTU_{L4\text{-}v} \rightarrow BU_{L\text{-}s}$	VT16278-F-300018
					VT16278-F-400006
					VT16278-F-400008
					VT49362-F-300001
					VT49362-F-300006
		$L\text{-}AOTU_{L} \rightarrow L\text{-}AOTU_{R}$	$L\text{-}AOTU_{L2\text{-}L3} \rightarrow L\text{-}AOTU_{R2\text{-}R3}$	$L\text{-}AOTU_{L2\text{-}L3} \rightarrow L\text{-}AOTU_{R2\text{-}R3}$	predicted
			$L\text{-}AOTU_{L3} \rightarrow L\text{-}AOTU_{R3}$	$L\text{-}AOTU_{L3} \rightarrow L\text{-}AOTU_{R3}$	predicted
VMP	VMP_{R}	$VMP_{R} \rightarrow BU_{RL}$::$L\text{-}AOTU_{RL}$	$VMP_{R\text{-}s} \rightarrow BU_{R\text{-}a,s,i,(L\text{-}a,s,i)}$::$L\text{-}AOTU_{R1\text{-}R4,L1\text{-}L4}$	$VMP_{R\text{-}s} \rightarrow BU_{R\text{-}a,s,i,(L\text{-}a,s,i)}$::$L\text{-}AOTU_{R1\text{-}R4,L1\text{-}L4}$	FCT_Trh-F-000082
	VMP_{L}	$VMP_{L} \rightarrow BU_{LR}$::$L\text{-}AOTU_{LR}$	$VMP_{L\text{-}s} \rightarrow BU_{L\text{-}a,s,i,(R\text{-}a,s,i)}$::$L\text{-}AOTU_{L1\text{-}L4,R1\text{-}R4}$	$VMP_{L\text{-}s} \rightarrow BU_{L\text{-}a,s,i,(R\text{-}a,s,i)}$::$L\text{-}AOTU_{L1\text{-}L4,R1\text{-}R4}$	FCT_VGlut-F-400630

Total types	94
Identified types	60
Predicted types	34
Prediction ratio	36 %

Synonym	*MC61	Otsuna et al. (2014)
	*MeTu	Omoto et al. (2017)
		Timaeus et al. (2020)
	**TuBu	Omoto et al. (2017)
		Timaeus et al. (2020)

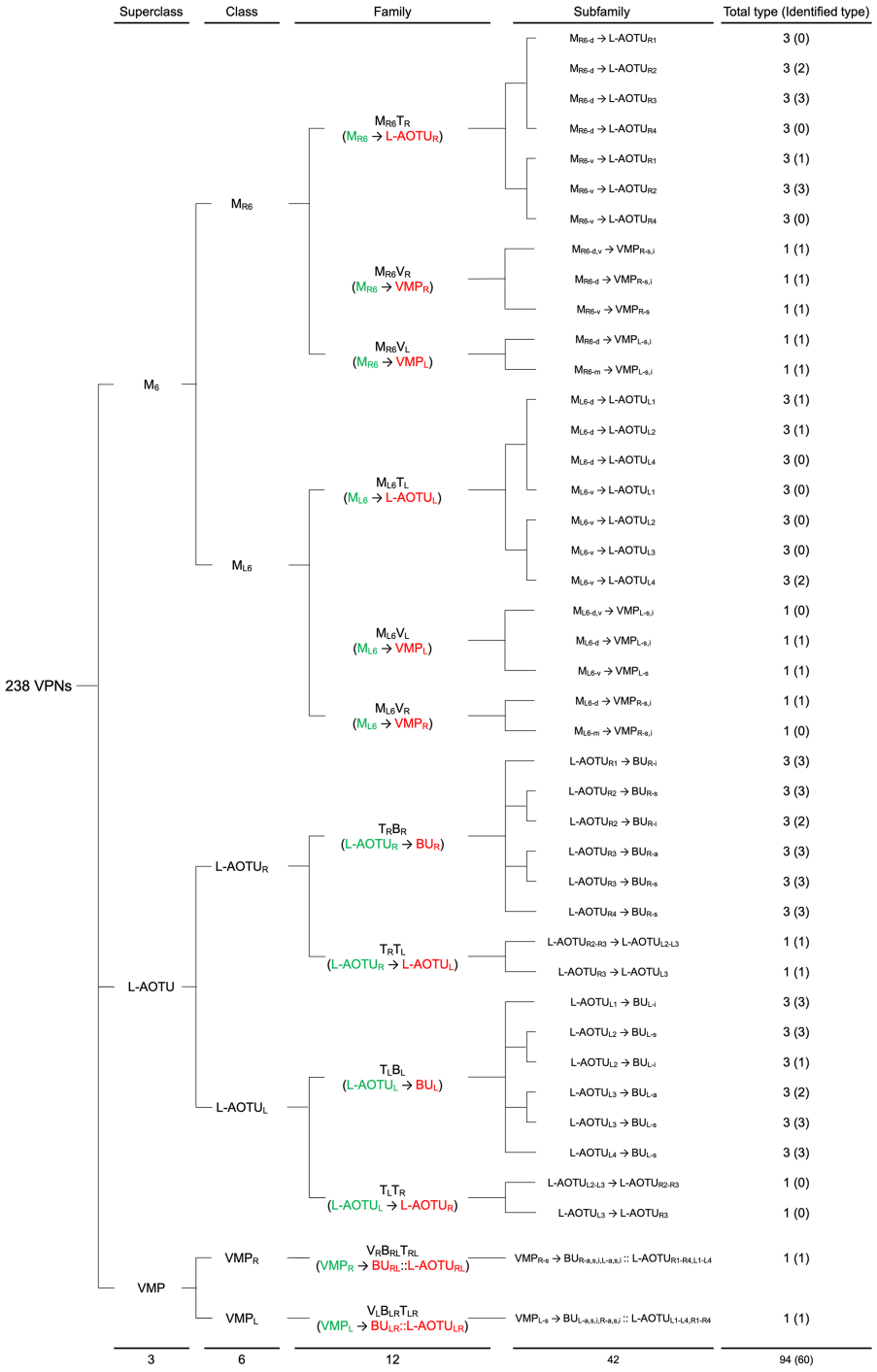

FIGURE 6 Classifying single visual projection neurons (VPNs) into 94 cell types (including 60 identified types). Classification tree diagram of 238 single visual projection neurons (VPNs). The arrow indicates the direction of the information flow. The regions where dendrites are located are shown in green and axons in red. The numbers in brackets indicate the types identified from our dataset of single neurons. M_6, medulla layer 6; L-AOTU, lateral anterior optic tubercle; VMP, ventral medial protocerebrum; BU, bulb; d, dorsal; m, medial; v, ventral; a, anterior; s, superior; l, inferior. See also Tables 3 and 4 [Color figure can be viewed at wileyonlinelibrary.com]

processes UV information in a multilayer, differential, and bilateral manner.

4.1 | Homologous VPNs in other insect species

We morphologically identified six groups of visual projection neurons (VPNs) that connect the optic lobe to the central brain in *Drosophila* (Figure 1b–g). Several VPNs presented in this study have been previously described in various insect species, including locust (Homberg et al., 2003), butterfly (Heinze et al., 2013), bee (Pfeiffer & Kinoshita, 2012; Zeller et al., 2015), and silk moth (Namiki & Kanzaki, 2018). After performing comparative analysis of the neuronal morphology in the identified M_6 downstream neurons, we provided a detailed list of the homologous VPNs in other insect species (Table 6). Three groups of VPNs are highly similar to the well-characterized polarization-sensitive neurons in locust (Homberg et al., 2003), butterfly (Heinze et al., 2013), and bees (Pfeiffer & Kinoshita, 2012; Zeller et al., 2015): (a) MT neurons are homologous to the

TABLE 4 Identified cell types (black) and predicted type from specific drivers (green) and symmetrical neuronal partner (red)

Superclass	Class	Family		Subfamily		Type		Identification			
		Name	Connection	Name	Connection	Name	Connection	Driver	Single neuron	Predicted	Single neuron no.
M_S	M_{R6}	$M_{R6}T_R$*	$M_{R6} \rightarrow$ L-AOTU$_R$*	$M_{R6\text{-}d}T_{R1}$	$M_{R6\text{-}d} \rightarrow$ L-AOTU$_{R1}$	$M_{R6\text{-}d}T_{R1\text{-}d}$	$M_{R6\text{-}d} \rightarrow$ L-AOTU$_{R1\text{-}d}$	●	○	●	0
						$M_{R6\text{-}d}T_{R1\text{-}m}$	$M_{R6\text{-}d} \rightarrow$ L-AOTU$_{R1\text{-}m}$	●	○	●	0
						$M_{R6\text{-}d}T_{R1\text{-}v}$	$M_{R6\text{-}d} \rightarrow$ L-AOTU$_{R1\text{-}v}$	●	○	●	0
				$M_{R6\text{-}d}T_{R2}$	$M_{R6\text{-}d} \rightarrow$ L-AOTU$_{R2}$	$M_{R6\text{-}d}T_{R2\text{-}d}$	$M_{R6\text{-}d} \rightarrow$ L-AOTU$_{R2\text{-}d}$	●	●	○	2
						$M_{R6\text{-}d}T_{R2\text{-}m}$	$M_{R6\text{-}d} \rightarrow$ L-AOTU$_{R2\text{-}m}$	●	●	○	3
						$M_{R6\text{-}d}T_{R2\text{-}v}$	$M_{R6\text{-}d} \rightarrow$ L-AOTU$_{R2\text{-}v}$	●	○	●	0
				$M_{R6\text{-}d}T_{R3}$	$M_{R6\text{-}d} \rightarrow$ L-AOTU$_{R3}$	$M_{R6\text{-}d}T_{R3\text{-}d}$	$M_{R6\text{-}d} \rightarrow$ L-AOTU$_{R3\text{-}d}$	●	●	○	12
						$M_{R6\text{-}d}T_{R3\text{-}m}$	$M_{R6\text{-}d} \rightarrow$ L-AOTU$_{R3\text{-}m}$	●	●	○	9
						$M_{R6\text{-}d}T_{R3\text{-}v}$	$M_{R6\text{-}d} \rightarrow$ L-AOTU$_{R3\text{-}v}$	●	●	○	1
				$M_{R6\text{-}d}T_{R4}$	$M_{R6\text{-}d} \rightarrow$ L-AOTU$_{R4}$	$M_{R6\text{-}d}T_{R4\text{-}d}$	$M_{R6\text{-}d} \rightarrow$ L-AOTU$_{R4\text{-}d}$	●	○	●	0
						$M_{R6\text{-}d}T_{R4\text{-}m}$	$M_{R6\text{-}d} \rightarrow$ L-AOTU$_{R4\text{-}m}$	●	○	●	0
						$M_{R6\text{-}d}T_{R4\text{-}v}$	$M_{R6\text{-}d} \rightarrow$ L-AOTU$_{R4\text{-}v}$	●	○	●	0
				$M_{R6\text{-}v}T_{R1}$	$M_{R6\text{-}v} \rightarrow$ L-AOTU$_{R1}$	$M_{R6\text{-}v}T_{R1\text{-}d}$	$M_{R6\text{-}v} \rightarrow$ L-AOTU$_{R1\text{-}d}$	●	○	●	0
						$M_{R6\text{-}v}T_{R1\text{-}m}$	$M_{R6\text{-}v} \rightarrow$ L-AOTU$_{R1\text{-}m}$	●	○	●	0
						$M_{R6\text{-}v}T_{R1\text{-}v}$	$M_{R6\text{-}v} \rightarrow$ L-AOTU$_{R1\text{-}v}$	●	●	○	1
				$M_{R6\text{-}v}T_{R2}$	$M_{R6\text{-}v} \rightarrow$ L-AOTU$_{R2}$	$M_{R6\text{-}v}T_{R2\text{-}d}$	$M_{R6\text{-}v} \rightarrow$ L-AOTU$_{R2\text{-}d}$	●	●	○	1
						$M_{R6\text{-}v}T_{R2\text{-}m}$	$M_{R6\text{-}v} \rightarrow$ L-AOTU$_{R2\text{-}m}$	●	●	○	1
						$M_{R6\text{-}v}T_{R2\text{-}v}$	$M_{R6\text{-}v} \rightarrow$ L-AOTU$_{R2\text{-}v}$	●	●	○	1
				$M_{R6\text{-}v}T_{R4}$	$M_{R6\text{-}v} \rightarrow$ L-AOTU$_{R4}$	$M_{R6\text{-}v}T_{R4\text{-}d}$	$M_{R6\text{-}v} \rightarrow$ L-AOTU$_{R4\text{-}d}$	●	○	●	0
						$M_{R6\text{-}v}T_{R4\text{-}m}$	$M_{R6\text{-}v} \rightarrow$ L-AOTU$_{R4\text{-}m}$	●	○	●	0
						$M_{R6\text{-}v}T_{R4\text{-}v}$	$M_{R6\text{-}v} \rightarrow$ L-AOTU$_{R4\text{-}v}$	●	○	●	0
		ipsilateral $M_R V_R$	$M_{R6} \rightarrow$ VMP$_R$	$M_{R6\text{-}d}V_{R\text{-}s.l}$	$M_{R6\text{-}d} \rightarrow$ VMP$_{R\text{-}s.l}$	$M_{R6\text{-}d}V_{R\text{-}s.l}$	$M_{R6\text{-}d} \rightarrow$ VMP$_{R\text{-}s.l}$	○	●	○	3
				$M_{R6\text{-}d}V_{R\text{-}s.l}$	$M_{R6\text{-}d} \rightarrow$ VMP$_{R\text{-}a.l}$	$M_{R6\text{-}d}V_{R\text{-}a.l}$	$M_{R6\text{-}d} \rightarrow$ VMP$_{R\text{-}a.l}$	○	●	○	13
				$M_{R6\text{-}v}V_{R\text{-}a}$	$M_{R6\text{-}v} \rightarrow$ VMP$_{R\text{-}a}$	$M_{R6\text{-}v}V_{R\text{-}a}$	$M_{R6\text{-}v} \rightarrow$ VMP$_{R\text{-}a}$	○	●	○	5
		contralateral $M_R V_L$	$M_{R6} \rightarrow$ VMP$_L$	$M_{R6\text{-}d}V_{L\text{-}a.l}$	$M_{R6\text{-}d} \rightarrow$ VMP$_{L\text{-}a.l}$	$M_{R6\text{-}d}V_{L\text{-}a.l}$	$M_{R6\text{-}d} \rightarrow$ VMP$_{L\text{-}a.l}$	○	●	○	1
				$M_{R6\text{-}d}V_{L\text{-}s.l}$	$M_{R6\text{-}m} \rightarrow$ VMP$_{L\text{-}s.l}$	$M_{R6\text{-}d}V_{L\text{-}s.l}$	$M_{R6\text{-}m} \rightarrow$ VMP$_{L\text{-}s.l}$	○	●	○	1
	M_{L6}	$M_L T_L$*	$M_{L6} \rightarrow$ L-AOTU$_L$*	$M_{L6\text{-}d}T_{L1}$	$M_{L6\text{-}d} \rightarrow$ L-AOTU$_{L1}$	$M_{L6\text{-}d}T_{L1\text{-}d}$	$M_{L6\text{-}d} \rightarrow$ L-AOTU$_{L1\text{-}d}$	●	○	●	0
						$M_{L6\text{-}d}T_{L1\text{-}m}$	$M_{L6\text{-}d} \rightarrow$ L-AOTU$_{L1\text{-}m}$	●	○	●	0
						$M_{L6\text{-}d}T_{L1\text{-}v}$	$M_{L6\text{-}d} \rightarrow$ L-AOTU$_{L1\text{-}v}$	●	●	○	1
				$M_{L6\text{-}d}T_{L2}$	$M_{L6\text{-}d} \rightarrow$ L-AOTU$_{L2}$	$M_{L6\text{-}d}T_{L2\text{-}d}$	$M_{L6\text{-}d} \rightarrow$ L-AOTU$_{L2\text{-}d}$	●	○	●	0
						$M_{L6\text{-}d}T_{L2\text{-}m}$	$M_{L6\text{-}d} \rightarrow$ L-AOTU$_{L2\text{-}m}$	●	●	○	1
						$M_{L6\text{-}d}T_{L2\text{-}v}$	$M_{L6\text{-}d} \rightarrow$ L-AOTU$_{L2\text{-}v}$	●	○	●	0
				$M_{L6\text{-}d}T_{L3}$	$M_{L6\text{-}d} \rightarrow$ L-AOTU$_{L3}$	$M_{L6\text{-}d}T_{L3\text{-}d}$	$M_{L6\text{-}v} \rightarrow$ L-AOTU$_{L2\text{-}d}$	●	●	○	19
						$M_{L6\text{-}d}T_{L3\text{-}m}$	$M_{L6\text{-}d} \rightarrow$ L-AOTU$_{L3\text{-}m}$	●	●	○	4
						$M_{L6\text{-}d}T_{L3\text{-}v}$	$M_{L6\text{-}d} \rightarrow$ L-AOTU$_{L3\text{-}v}$	●	●	○	4
				$M_{L6\text{-}d}T_{L4}$	$M_{L6\text{-}d} \rightarrow$ L-AOTU$_{L4}$	$M_{L6\text{-}d}T_{L4\text{-}d}$	$M_{L6\text{-}d} \rightarrow$ L-AOTU$_{L4\text{-}d}$	●	○	●	0
						$M_{L6\text{-}d}T_{L4\text{-}m}$	$M_{L6\text{-}d} \rightarrow$ L-AOTU$_{L4\text{-}m}$	●	○	●	0
						$M_{L6\text{-}d}T_{L4\text{-}v}$	$M_{L6\text{-}d} \rightarrow$ L-AOTU$_{L4\text{-}v}$	●	○	●	0
				$M_{L6\text{-}v}T_{L1}$	$M_{L6\text{-}v} \rightarrow$ L-AOTU$_{L1}$	$M_{L6\text{-}v}T_{L1\text{-}d}$	$M_{L6\text{-}v} \rightarrow$ L-AOTU$_{L1\text{-}d}$	●	○	●	0
						$M_{L6\text{-}v}T_{L1\text{-}m}$	$M_{L6\text{-}v} \rightarrow$ L-AOTU$_{L1\text{-}m}$	●	○	●	0
						$M_{L6\text{-}v}T_{L1\text{-}v}$	$M_{L6\text{-}v} \rightarrow$ L-AOTU$_{L1\text{-}v}$	●	○	●	0
				$M_{L6\text{-}v}T_{L2}$	$M_{L6\text{-}v} \rightarrow$ L-AOTU$_{L2}$	$M_{L6\text{-}v}T_{L2\text{-}d}$	$M_{L6\text{-}v} \rightarrow$ L-AOTU$_{L2\text{-}d}$	●	○	●	0
						$M_{L6\text{-}v}T_{L2\text{-}m}$	$M_{L6\text{-}v} \rightarrow$ L-AOTU$_{L2\text{-}m}$	●	○	●	0
						$M_{L6\text{-}v}T_{L2\text{-}v}$	$M_{L6\text{-}v} \rightarrow$ L-AOTU$_{L2\text{-}v}$	●	○	●	0
				$M_{L6\text{-}v}T_{L4}$	$M_{L6\text{-}v} \rightarrow$ L-AOTU$_{L4}$	$M_{L6\text{-}v}T_{L4\text{-}d}$	$M_{L6\text{-}v} \rightarrow$ L-AOTU$_{L4\text{-}d}$	●	●	○	2
						$M_{L6\text{-}v}T_{L4\text{-}m}$	$M_{L6\text{-}v} \rightarrow$ L-AOTU$_{L4\text{-}m}$	●	●	○	1
						$M_{L6\text{-}v}T_{L4\text{-}v}$	$M_{L6\text{-}v} \rightarrow$ L-AOTU$_{L4\text{-}v}$	●	○	●	0
		ipsilateral $M_L V_L$	$M_{L6} \rightarrow$ VMP$_L$	$M_{L6\text{-}d}V_{L\text{-}s.l}$	$M_{L6\text{-}d} \rightarrow$ VMP$_{L\text{-}s.l}$	$M_{L6\text{-}d}V_{L\text{-}s.l}$	$M_{L6\text{-}d} \rightarrow$ VMP$_{L\text{-}s.l}$	○	○	●	0
				$M_{L6\text{-}d}V_{L\text{-}s.l}$	$M_{L6\text{-}d} \rightarrow$ VMP$_{L\text{-}s.l}$	$M_{L6\text{-}d}V_{L\text{-}s.l}$	$M_{L6\text{-}d} \rightarrow$ VMP$_{L\text{-}s.l}$	○	●	○	16
				$M_{L6\text{-}v}V_{L\text{-}s}$	$M_{L6\text{-}v} \rightarrow$ VMP$_{L\text{-}s}$	$M_{L6\text{-}v}V_{L\text{-}s}$	$M_{L6\text{-}v} \rightarrow$ VMP$_{L\text{-}s}$	○	●	○	1
		contralateral $M_L V_R$	$M_{L6} \rightarrow$ VMP$_R$	$M_{L6\text{-}d}V_{R\text{-}s.l}$	$M_{L6\text{-}d} \rightarrow$ VMP$_{R\text{-}s.l}$	$M_{L6\text{-}d}V_{R\text{-}s.l}$	$M_{L6\text{-}d} \rightarrow$ VMP$_{R\text{-}s.l}$	○	●	○	2
				$M_{L6\text{-}d}V_{R\text{-}s.l}$	$M_{L6\text{-}m} \rightarrow$ VMP$_{R\text{-}s.l}$	$M_{L6\text{-}d}V_{R\text{-}s.l}$	$M_{L6\text{-}m} \rightarrow$ VMP$_{R\text{-}s.l}$	○	○	●	0
L-AOTU	L-AOTU$_R$	$T_R B_R$**	L-AOT$_R \rightarrow$ BU$_R$**	$T_{R1}B_{R4}$	L-AOTU$_{R1} \rightarrow$ BU$_{R4}$	$T_{R1\text{-}d}B_{R4}$	L-AOTU$_{R1\text{-}d} \rightarrow$ BU$_{R4}$	●	●	○	2
						$T_{R1\text{-}m}B_{R4}$	L-AOTU$_{R1\text{-}m} \rightarrow$ BU$_{R4}$	●	●	○	2
						$T_{R1\text{-}v}B_{R4}$	L-AOTU$_{R1\text{-}v} \rightarrow$ BU$_{R4}$	●	●	○	8

TABLE 4 Continued

				$T_{R2}B_{R-s}$	L-AOTU$_{R2}$ → BU$_{R-s}$	$T_{R2-d}B_{R-s}$	L-AOTU$_{R2-d}$ → BU$_{R-s}$	●	●	○	6
						$T_{R2-m}B_{R-s}$	L-AOTU$_{R2-m}$ → BU$_{R-s}$	●	●	○	4
						$T_{R2-v}B_{R-s}$	L-AOTU$_{R2-v}$ → BU$_{R-s}$	●	●	○	4
				$T_{R2}B_{R-i}$	L-AOTU$_{R2}$ → BU$_{R-i}$	$T_{R2-d}B_{R-i}$	L-AOTU$_{R2-d}$ → BU$_{R-i}$	●	○	●	0
						$T_{R2-m}B_{R-i}$	L-AOTU$_{R2-m}$ → BU$_{R-i}$	●	●	○	2
						$T_{R2-v}B_{R-i}$	L-AOTU$_{R2-v}$ → BU$_{R-i}$	●	●	○	1
				$T_{R3}B_{R-s}$	L-AOTU$_{R3}$ → BU$_{R-s}$	$T_{R3-d}B_{R-s}$	L-AOTU$_{R3-d}$ → BU$_{R-s}$	●	●	○	1
						$T_{R3-m}B_{R-s}$	L-AOTU$_{R3-m}$ → BU$_{R-s}$	●	●	○	5
						$T_{R3-v}B_{R-s}$	L-AOTU$_{R3-v}$ → BU$_{R-s}$	●	●	○	3
				$T_{R3}B_{R-s}$	L-AOTU$_{R3}$ → BU$_{R-s}$	$T_{R3-d}B_{R-s}$	L-AOTU$_{R3-d}$ → BU$_{R-s}$	●	●	○	1
						$T_{R3-m}B_{R-s}$	L-AOTU$_{R3-m}$ → BU$_{R-s}$	●	●	○	4
						$T_{R3-v}B_{R-s}$	L-AOTU$_{R3-v}$ → BU$_{R-s}$	●	●	○	14
				$T_{R4}B_{R-s}$	L-AOTU$_{R4}$ → BU$_{R-s}$	$T_{R4-d}B_{R-s}$	L-AOTU$_{R4-d}$ → BU$_{R-s}$	●	●	○	3
						$T_{R4-m}B_{R-s}$	L-AOTU$_{R4-m}$ → BU$_{R-s}$	●	●	○	3
						$T_{R4-v}B_{R-s}$	L-AOTU$_{R4-v}$ → BU$_{R-s}$	●	●	○	6
		T_RT_L	L-AOTU$_R$ → L-AOTU$_L$	$T_{R2-R3}T_{L2-L3}$	L-AOTU$_{R2-R3}$ → L-AOTU$_{L2-L3}$	$T_{R2-R3}T_{L2-L3}$	L-AOTU$_{R2-R3}$ → L-AOTU$_{L2-L3}$	●	●	○	3
				$T_{R3}T_{L3}$	L-AOTU$_{R3}$ → L-AOTU$_{L3}$	$T_{R3}T_{L3}$	L-AOTU$_{R3}$ → L-AOTU$_{L3}$	●	●	○	2
						$T_{L1-d}B_{L-i}$	L-AOTU$_{L1-d}$ → BU$_{L-i}$	●	●	○	1
				$T_{L1}B_{L-i}$	L-AOTU$_{L1}$ → BU$_{L-i}$	$T_{L1-m}B_{L-i}$	L-AOTU$_{L1-m}$ → BU$_{L-i}$	●	●	○	2
						$T_{L1-v}B_{L-i}$	L-AOTU$_{L1-v}$ → BU$_{L-i}$	●	●	○	8
						$T_{L2-d}B_{L-s}$	L-AOTU$_{L2-d}$ → BU$_{L-s}$	●	●	○	4
				$T_{L2}B_{L-s}$	L-AOTU$_{L2}$ → BU$_{L-s}$	$T_{L2-m}B_{L-s}$	L-AOTU$_{L2-m}$ → BU$_{L-s}$	●	●	○	5
						$T_{L2-v}B_{L-s}$	L-AOTU$_{L2-v}$ → BU$_{L-s}$	●	●	○	6
L-AOTU$_L$		T_LB_L**	L-AOTU$_L$ → BU$_L$**			$T_{L2-d}B_{L-i}$	L-AOTU$_{L2-d}$ → BU$_{L-i}$	●	○	●	0
				$T_{L2}B_{L-i}$	L-AOTU$_{L2}$ → BU$_{L-i}$	$T_{L2-m}B_{L-i}$	L-AOTU$_{L2-m}$ → BU$_{L-i}$	●	●	○	2
						$T_{L2-v}B_{L-i}$	L-AOTU$_{L2-v}$ → BU$_{L-i}$	●	○	●	0
						$T_{L3-d}B_{L-s}$	L-AOTU$_{L3-d}$ → BU$_{L-s}$	●	○	●	0
				$T_{L3}B_{L-s}$	L-AOTU$_{L3}$ → BU$_{L-s}$	$T_{L3-m}B_{L-s}$	L-AOTU$_{L3-m}$ → BU$_{L-s}$	●	●	○	1
						$T_{L3-v}B_{L-s}$	L-AOTU$_{L3-v}$ → BU$_{L-s}$	●	●	○	1
						$T_{L3-m}B_{L-s}$	L-AOTU$_{L3-m}$ → BU$_{L-s}$	●	●	○	4
						$T_{L3-v}B_{L-s}$	L-AOTU$_{L3-v}$ → BU$_{L-s}$	●	●	○	14
						$T_{L4-d}B_{L-s}$	L-AOTU$_{L4-d}$ → BU$_{L-s}$	●	●	○	1
				$T_{L4}B_{L-s}$	L-AOTU$_{L4}$ → BU$_{L-s}$	$T_{L4-m}B_{L-s}$	L-AOTU$_{L4-m}$ → BU$_{L-s}$	●	●	○	1
						$T_{L4-v}B_{L-s}$	L-AOTU$_{L4-v}$ → BU$_{L-s}$	●	●	○	5
		T_LT_R	L-AOTU$_L$ → L-AOTU$_R$	$T_{L2-L3}T_{R2-R3}$	L-AOTU$_{L2-L3}$ → L-AOTU$_{R2-R3}$	$T_{L2-L3}T_{R2-R3}$	L-AOTU$_{L2-L3}$ → L-AOTU$_{R2-R3}$	●	○	●	0
				$T_{L3}T_{R3}$	L-AOTU$_{L3}$ → L-AOTU$_{R3}$	$T_{L3}T_{R3}$	L-AOTU$_{L3}$ → L-AOTU$_{R3}$	●	○	●	0
VMP	VMP$_R$	$V_RB_{RL}T_{RL}$	VMP$_R$ → BU$_{RL}$::L-AOTU$_{RL}$	$V_{R-s}B_{R-s,(L-s,L-i)}T_{R1-R4,L1-L4}$	VMP$_{R-s}$ → BU$_{R-s,(L-s,L-i)}$::L-AOTU$_{R1-R4,L1-L4}$	$V_{R-s}B_{R-s,(L-s,L-i)}T_{R1-R4,L1-L4}$	VMP$_{R-s}$ → BU$_{R-s,(L-s,L-i)}$::L-AOTU$_{R1-R4,L1-L4}$	○	●	○	1
	VMP$_L$	$V_LB_{LR}T_{LR}$	VMP$_L$ → BU$_{LR}$::L-AOTU$_{LR}$	$V_{L-s}B_{L-s,(R-s,R-i)}T_{L1-L4,R1-R4}$	VMP$_{L-s}$ → BU$_{L-s,(R-s,R-i)}$::L-AOTU$_{L1-L4,R1-R4}$	$V_{L-s}B_{L-s,(R-s,R-i)}T_{L1-L4,R1-R4}$	VMP$_{L-s}$ → BU$_{L-s,(R-s,R-i)}$::L-AOTU$_{L1-L4,R1-R4}$	○	●	○	1
Superclass	**Class**	**Family**		**Subfamily**		**Type**	**Predicted type**	**†Prediction ratio**			**Single neuron no.**
3	6	12		42		94	34	36 %			238

Synonym	*MC61	Otsuna et al. (2014)
	*MeTu	Omoto et al. (2017)
		Timaeus et al. (2020)
	**TuBu	Omoto et al. (2017)
		Timaeus et al. (2020)

[a]Neuronal types are predicted from the specific drivers are shown in green (prediction ratio: 34%) and from the symmetrical neuronal partner are shown in red (Prediction ratio: 2%).

transmedullary (TM) neurons with dendritic arbors in the medulla and axon terminals in the lower AOTU; (b) TB neurons are homologous to the tubercle-accessory lobe 1 (TuLAL1) neurons with dendritic arbors in the lower AOTU and axon terminals in the lateral and medial bulb; and (c) TT neurons are homologous to the tubercle-tubercle neuron 1 (TuTu1) neurons connecting the lower AOTUs of both hemispheres via the intertubercle tract. TT neurons in the fly are likely to be involved in polarization and color vision, as suggested by the functional studies of the TuTu1 neurons in the locust. Based on the size and location related to the surrounding neuropils, the VMP of the fly resembles the posterior slope of the silk moth. Thus, the ipsilateral MV neurons in *Drosophila* may also be involved in the mating behavior, as demonstrated in the morphologically similar medulla output neurons of the silk moth (Namiki & Kanzaki, 2018). With these anatomical observations, it can be stated that most of the visual projection neurons are highly conserved in different insect species (Kinoshita et al., 2007; Pfeiffer & Homberg, 2007).

TABLE 5 Lookup table of neuropil abbreviations

M_6	**Medulla, layer 6**	**L-AOTU$_{L1-m}$**	**Left L-AOTU, 1st column, medial glomerulus**
M_{R6}	Right M_6	**L-AOTU$_{L1-v}$**	Left L-AOTU, 1st column, ventral glomerulus
M_{R6-d}	Right M_6, dorsal part	**L-AOTU$_{L2}$**	Left L-AOTU, 2nd column
M_{R6-m}	Right M_6, medial part	**L-AOTU$_{L2-d}$**	Left L-AOTU, 2nd column, dorsal glomerulus
M_{R6-v}	Right M_6, ventral part	**L-AOTU$_{L2-m}$**	Left L-AOTU, 2nd column, medial glomerulus
M_{L6}	Left M_6	**L-AOTU$_{L2-v}$**	Left L-AOTU, 2nd column, ventral glomerulus
M_{L6-d}	Left M_6, dorsal part	**L-AOTU$_{L3}$**	Left L-AOTU, 3rd column
M_{L6-m}	Left M_6, medial part	**L-AOTU$_{L3-d}$**	Left L-AOTU, 3rd column, dorsal glomerulus
M_{L6-v}	Left M_6, ventral part	**L-AOTU$_{L3-m}$**	Left L-AOTU, 3rd column, medial glomerulus
L-AOTU	Lateral Anterior Optic Tubercle	**L-AOTU$_{L3-v}$**	Left L-AOTU, 3rd column, ventral glomerulus
L-AOTU$_R$	Right L-AOTU	**L-AOTU$_{L4}$**	Left L-AOTU, 4th column
L-AOTU$_{R1}$	Right L-AOTU, 1st column	**L-AOTU$_{L4-d}$**	Left L-AOTU, 4th column, dorsal glomerulus
L-AOTU$_{R1-d}$	Right L-AOTU, 1st column, dorsal glomerulus	**L-AOTU$_{L4-m}$**	Left L-AOTU, 4th column, medial glomerulus
L-AOTU$_{R1-m}$	Right L-AOTU, 1st column, medial glomerulus	**L-AOTU$_{L4-v}$**	Left L-AOTU, 4th column, ventral glomerulus
L-AOTU$_{R1-v}$	Right L-AOTU, 1st column, ventral glomerulus	**BU**	Bulb
L-AOTU$_{R2}$	Right L-AOTU, 2nd column	**BU$_R$**	Right BU
L-AOTU$_{R2-d}$	Right L-AOTU, 2nd column, dorsal glomerulus	**BU$_{R-a}$**	Right BU, anterior group
L-AOTU$_{R2-m}$	Right L-AOTU, 2nd column, medial glomerulus	**BU$_{R-s}$**	Right BU, superior group
L-AOTU$_{R2-v}$	Right L-AOTU, 2nd column, ventral glomerulus	**BU$_{R-i}$**	Right BU, inferior group
L-AOTU$_{R3}$	Right L-AOTU, 3rd column	**BU$_L$**	Left BU
L-AOTU$_{R3-d}$	Right L-AOTU, 3rd column, dorsal glomerulus	**BU$_{L-a}$**	Left BU, anterior group
L-AOTU$_{R3-m}$	Right L-AOTU, 3rd column, medial glomerulus	**BU$_{L-s}$**	Left BU, superior group
L-AOTU$_{R3-v}$	Right L-AOTU, 3rd column, ventral glomerulus	**BU$_{L-i}$**	Left BU, inferior group
L-AOTU$_{R4}$	Right L-AOTU, 4th column	**VMP**	Ventral Medial Protocerebrum
L-AOTU$_{R4-d}$	Right L-AOTU, 4th column, dorsal glomerulus	**VMP$_R$**	Right VMP
L-AOTU$_{R4-m}$	Right L-AOTU, 4th column, medial glomerulus	**VMP$_{R-s}$**	Right VMP, superior part
L-AOTU$_{R4-v}$	Right L-AOTU, 4th column, ventral glomerulus	**VMP$_{R-i}$**	Right VMP, inferior part
L-AOTU$_L$	Left L-AOTU	**VMP$_L$**	Left VMP
L-AOTU$_{L1}$	Left L-AOTU, 1st column	**VMP$_{L-s}$**	Left VMP, superior part
L-AOTU$_{L1-d}$	Left L-AOTU, 1st column, dorsal glomerulus	**VMP$_{L-i}$**	Left VMP, inferior part

4.2 | Internal representation of UV information at the L-AOTU

Three independent lines of evidence showed that each L-AOTU consisted of four columns, and every column consisted of three glomeruli: (a) evident anatomical boundary revealed by DLG immunostaining; (b) column-specific Gal4 and LexA expression; and (c) single glomerulus-specific input MT neurons and output TB neurons.

As each UV-sensing R7 neuron had an axonal bouton in a single M_6 column, the terminals of all the R7 neurons of ~750 ommatidia form a retinotopic map at the M_6 in a one-to-one pattern (Chin et al., 2014). The stereotypical connectivity of single MT neurons suggested the second layer of the internal representation of UV information to the 12 L-AOTU glomeruli. As a single MT neuron had a dendritic arbor covering approximately 30 M_6 columns and an axon terminal in one L-AOTU glomerulus, an internal representation of UV information at the L-AOTU required at least 25 MT neurons (Figure 12). However, a L-AOTU single column-specific driver was expressed in 10–80 MT neurons with dendritic arbors covering both dorsal and ventral M_6, suggesting that each L-AOTU column received UV information from the entire visual field (Figure 13). Thus, a L-AOTU glomerulus may receive inputs from at least 8 MT neurons relaying UV information from approximately 250 M_6 columns. Altogether, the M_6 representation of the anterior–posterior visual field is likely further represented by the MT neurons along the dorsal–ventral axis of the three glomeruli in each L-AOTU column. The calcium response of MT downstream neurons, that is, TB neurons and ring neurons of the EB, to horizontally moving objects suggested that each of the four L-AOTU columns may separately be involved in processing azimuth of the visual field (Seelig & Jayaraman, 2013; Omoto et al., 2017).

The differential role of the four L-AOTU columns remains unclear. Previous studies revealed three L-AOTU columns: the medial L-AOTU, the intermediate lateral L-AOTU, and the lateral L-

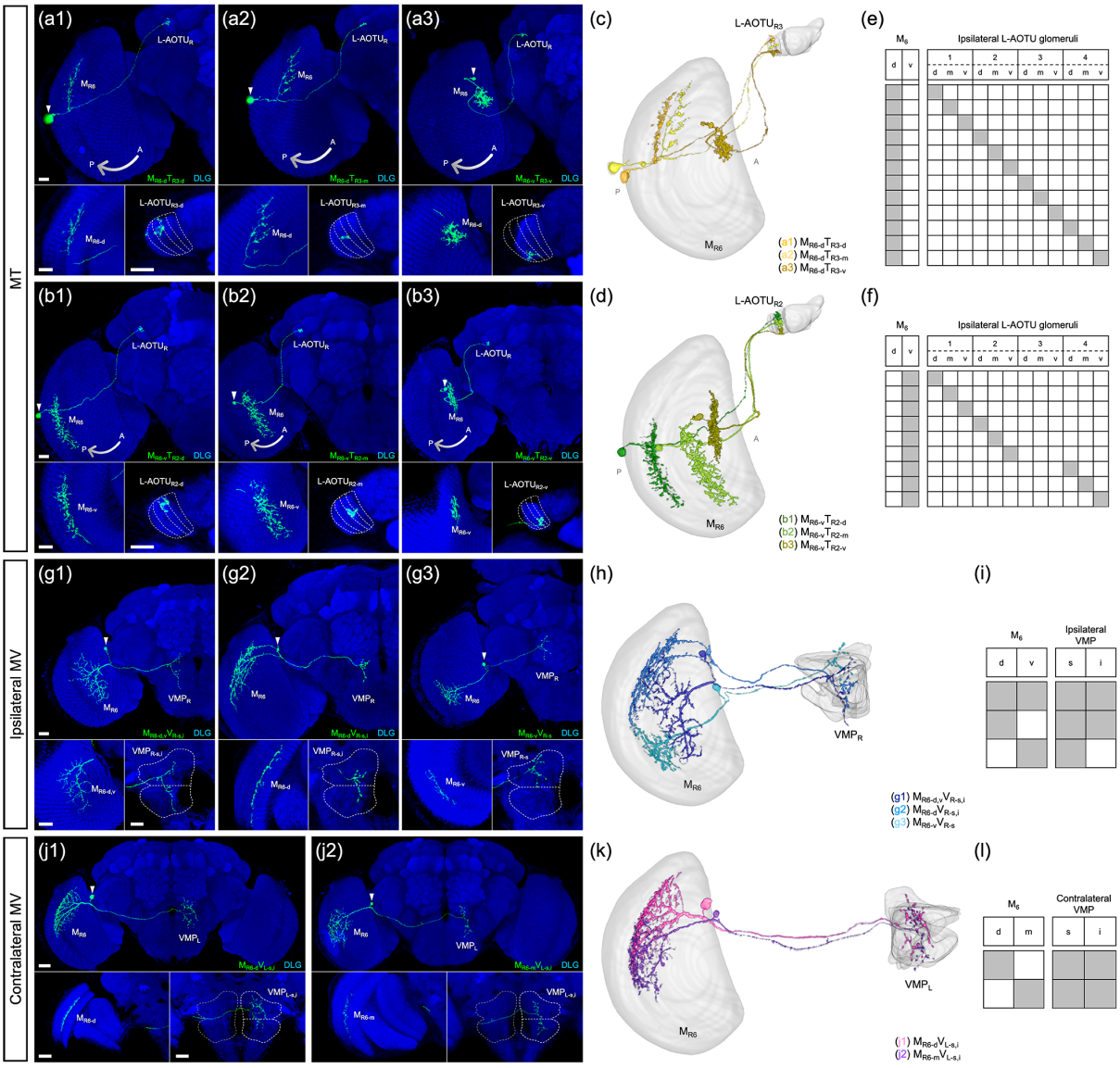

FIGURE 7 Connectivity analysis for medulla layer 6 (M_6) output neurons MT, ipsilateral MV, and contralateral MV. (a) Three representative MT neurons of the $M_{R6\text{-}d}T_{R3}$ subfamily. (b) Three representative MT neurons of the $M_{R6\text{-}v}T_{R2}$ subfamily. Brain structures immunostained with anti-DLG antibodies (blue). (c–d) Spatial distributions of three representative MT neurons of the same subfamily. Each MT neuron is registered to a standard brain and is shown in a different color. (e–f) Gray indicates the innervation patterns of MT neurons between medulla layer 6 (M_6) domains and lateral anterior optic tubercle (L-AOTU) glomeruli. (g) Three representative ipsilateral MV neurons of different subfamilies. Brain structures immunostained with anti-DLG antibodies (blue). (h) Spatial distribution of three representative ipsilateral MV neurons of different subfamilies. Each ipsilateral MV neuron is registered to a standard brain and shown in a different color. (i) Gray indicates the innervation patterns of MV neurons between M_6 domains and ipsilateral ventral medial protocerebrum (VMP) domains. (j) Two representative contralateral MV neurons of different subfamilies. Brain structures immunostained with anti-DLG antibodies (blue). (k) Spatial distribution of two representative contralateral MV neurons of different subfamilies. Each contralateral MV neuron is registered to a standard brain and shown in a different color. (l) Gray indicates the innervation patterns of contralateral MV neurons between M_6 domains and contralateral VMP domains. Images are frontal views of confocal projections of several adjacent optical sections unless otherwise specified. Scale bars: 20 μm [Color figure can be viewed at wileyonlinelibrary.com]

AOTU (Omoto et al., 2017; Timaeus et al., 2020). With the single column-specific driver expression and glomerulus-specific single neuron morphology, we showed that the intermediate lateral L-AOTU consists of two columns. Intriguingly, commissural TT neurons connected only the two middle columns between the two brain hemispheres. Similar commissural neurons were shown to be sensitive to polarized light, unpolarized light, and UV/green opponency in the locust brain (Kinoshita et al., 2007; Pfeiffer & Homberg, 2007). The distinct connectivity of individual TB neurons between single L-AOTU glomeruli and single BU microglomeruli further supported the differential role of the four L-AOTU columns. Moreover, functional imaging showed that the BU_s are sensitive to stimuli from the ipsilateral visual field and the BU_i to stimuli from the contralateral visual field (Omoto et al., 2017). Altogether, these results suggested that every L-AOTU column receives inputs from the entire ipsilateral visual

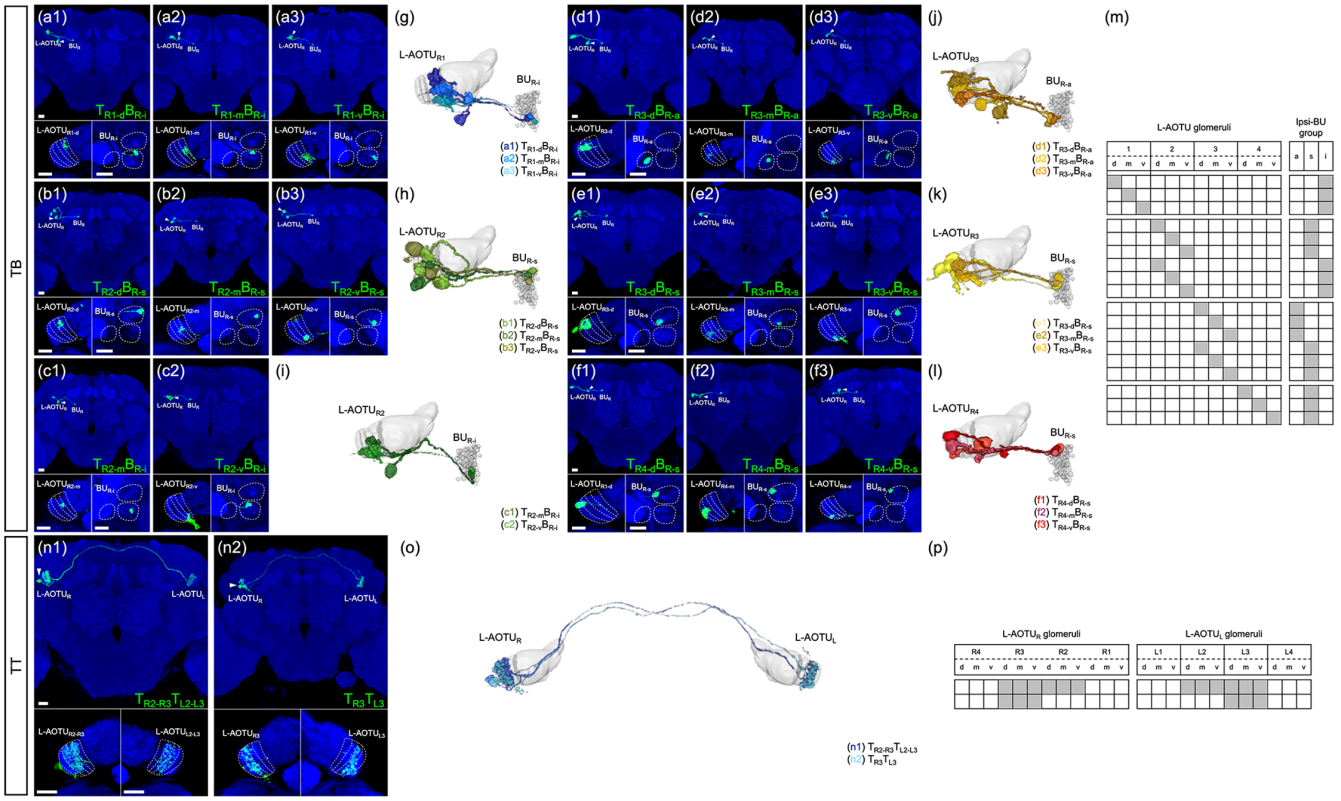

FIGURE 8 Connectivity analysis for lateral anterior optic tubercle (L-AOTU) output neurons TB and TT. (a) Three representative TB neurons of the $T_{R1}B_{R\text{-}i}$ subfamily. (b) Three representative TB neurons of the $T_{R2}B_{R\text{-}s}$ subfamily. (c) Two representative TB neurons of the $T_{R2}B_{R\text{-}i}$ subfamily. (d) Three representative TB neurons of the $T_{R3}B_{R\text{-}a}$ subfamily. (e) Three representative TB neurons of the $T_{R3}B_{R\text{-}s}$ subfamily. (f) Three representative TB neurons of the $T_{R4}B_{R\text{-}s}$ subfamily. Brain structures immunostained with anti-DLG antibodies (blue). (g–l) Spatial distribution of three representative TB neurons of the same subfamily. Each TB neuron is registered to a standard brain and shown in a different color. (m) Gray indicates the innervation patterns of the TB neurons between L-AOTU glomeruli and ipsilateral BU groups. (n) Two representative TT neurons of different subfamilies. Brain structures immunostained with anti-DLG antibodies (blue). (o) Spatial distribution of two representative TT neurons of the different subfamilies. Each TT neuron is registered to a standard brain and shown in a different color. (p) Gray indicates the innervation patterns of the TT neurons between the right and left L-AOTU glomeruli. Images are mostly frontal views of confocal projections of several adjacent optical sections unless otherwise specified. Scale bars: 20 μm [Color figure can be viewed at wileyonlinelibrary.com]

field. However, only the two middle L-AOTU columns also receive inputs from the contralateral visual field, suggesting a differential role of the four L-AOTU columns in the integration of UV information from the two eyes.

Furthermore, we predicted additional 34 types of M_6 downstream neurons by examining thousands of single-neuron images and driver expressions (See Table 4 for the list of predicted cell types in each family). These predicted neurons can be grouped into two groups comprised 32 and two cell types that were predicted from the specific drivers and the symmetrical neuronal partner, respectively. However, it should be noted that the neuronal types in each family might be incomplete, although we described a large number of visual projection neurons in this study. Neuronal types that connect L-AOTU$_1$ and L-AOTU$_3$ bilaterally across the two hemispheres may exist, as it has been shown that in honeybees, all compartments of the AOTUs of both hemispheres are connected via three types of TT neurons (Zeller et al., 2015). Our light microscopy data with electron microscopy reconstructions of the entire adult fruit fly brain could help to map the complete population of these visual projection neurons (Zheng et al., 2018).

4.3 | Parallel processing and bilateral integration

Parallel circuit processing is a common feature of most sensory modalities, such as the visual and olfactory sensory systems. In *Drosophila*, the olfactory projection neurons relaying odor information to the mushroom body and the lateral horn were proposed to mediate learned and innate olfactory behaviors, respectively (Amin & Lin, 2019; Sanes & Zipursky, 2010). The M_6 → L-AOTU → EB is a common pathway processing polarized light for decision-making during navigation in insects (el Jundi et al., 2014; Warren et al., 2019). Here, we found another pathway M_6 → VMP with MV neurons relaying M_6 information directly to the VMP premotor center, where dense descending neurons link the brain to the ventral nerve cord for rapid locomotion response (Namiki et al., 2018). In the silk moth *Bombyx mori*, head orientation requires a visual

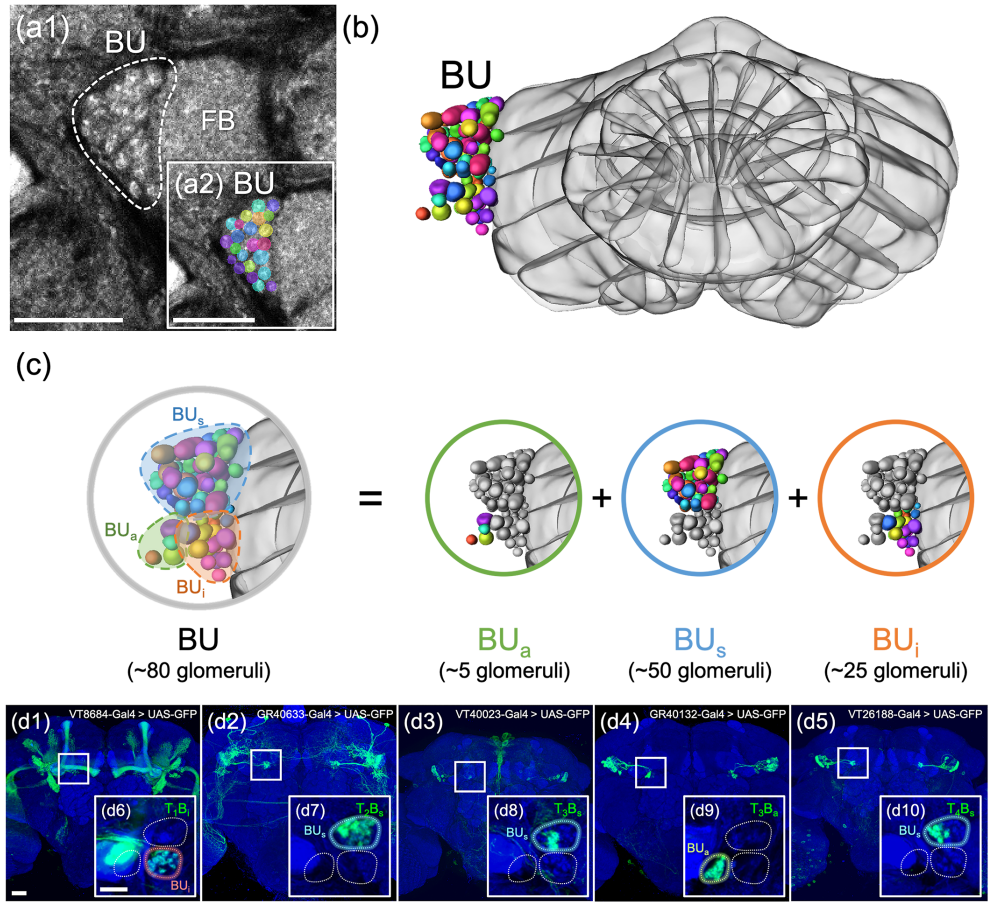

FIGURE 9 The bulb (BU) consists of ~80 microglomeruli divided into three groups. (a1) The bulb (BU) is located in the central brain at the side of the fan-shaped body (FB). (a2) Imaging of anti-discs large (DLG) stained neuropils (gray) reveals clear structural boundaries, including the granular structure of BU. Each color reveals a demarcated substructure in the BU. (b) Volume models of 80 microglomeruli in the BU. (c) Volume models of BU groups: The anterior group (BU$_a$), the superior group (BU$_s$), and the inferior (BU$_i$) group. (d1–d5) Expression of column-specific Gal4 drivers in TB that were visualized with mCD8::GFP. (e5–e8) High-magnification image in the BU groups of TB neurons (boxed inset). Brain structures immunostained with anti-DLG antibodies (blue). Images are mostly frontal views of confocal projections of several adjacent optical sections unless otherwise specified. a, anterior; s, superior; i, inferior. Scale bars: 20 μm [Color figure can be viewed at wileyonlinelibrary.com]

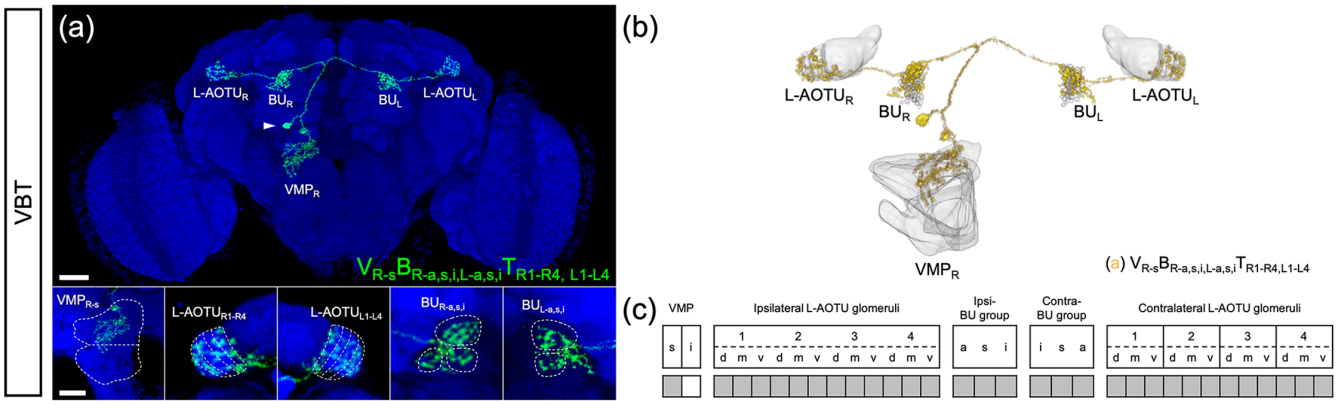

FIGURE 10 Connectivity analysis for ventral medial protocerebrum (VMP) output neurons VBT. (a) A representative VBT neuron (green). Brain structures immunostained with anti-DLG antibodies (blue). (b) The VBT neuron is registered to a standard brain. (c) Gray indicates the innervation patterns of VBT neurons between VMP domains, L-AOTU glomeruli, and BU groups. Images are frontal views of confocal projections of several adjacent optical sections unless otherwise specified. scale bars: 20 μm [Color figure can be viewed at wileyonlinelibrary.com]

TABLE 6 Lookup table of homologous visual projection neurons across species

Fruit fly			Locust, monarch butterfly, bumblebee, honeybee, silk moth	
Neuron name in the current study	**Other name in the literatures**	**Reference**	**Homologous neurons in other species**	**Reference**
MT (M_6 → L-AOTU)	**MeTu** (medullo-tubercular neurons)	Omoto et al. (2017)	**TM** (transmedullary neurons)	**Locust**: Homberg et al. (2003)
		Timaeus et al. (2020)		**Butterfly**: Heinze et al. (2013)
	MC61 (medullar columnar 61 neurons)	Otsuna et al. (2014)		**Bumblebee**: Pfeiffer and Kinoshita (2012)
	TM (transmedullary neurons)	Fischbach and Dittrich (1989)		**Honeybee**: Zeller et al. (2015)
TB (L-AOTU → BU)	**TuBu** (tubercular-bulbar neurons)	Omoto et al. (2017)	**TuLAL1** (tubercle-accessory lobe 1 neurons)	**Locust**: Homberg et al. (2003)
		Timaeus et al. (2020)		**Butterfly**: Heinze et al. (2013)
		Lamaze et al. (2018)		**Bumblebee**: Pfeiffer and Kinoshita (2012)
		Guo et al. (2018)		**Honeybee**: Zeller et al. (2015)
TT (L-AOTU → L-AOTU)	–	–	**TuTu1** (tubercle-tubercle neuron 1 neurons)	**Locust**: Homberg et al. (2003)
				Butterfly: Heinze et al. (2013)
				Bumblebee: Pfeiffer and Kinoshita (2012)
				Honeybee: Zeller et al. (2015)
ipsilateral MV (M_6 → ipsi-VMP)	–	–	Medulla output neurons (unnamed)	**Silk moth**: Namiki and Kanzaki (2018)

TABLE 7 List of ellipsoid body (EB) ring neuron types

	Innervation			
Neuron type	**EB rings**[a]	**BU groups**[b]	**Neurotransmitter**	**Reference**
R1	C	i	GABA	Hanesch et al. (1989)
			Glutamate	Daniels et al. (2008)
			Acetylcholine	Zhang et al. (2013)
R2	A	s	GABA	Hanesch et al. (1989)
			Acetylcholine	Zhang et al. (2013)
R3	A	i	GABA	Hanesch et al. (1989)
			Glutamate	Daniels et al. (2008)
R4d	O	s	GABA	Hanesch et al. (1989)
R4m	O	a, s	GABA	Hanesch et al. (1989)
			Glutamate	RW Daniels et al. (2008)
			Acetylcholine	Zhang et al. (2013)
P	P	–	–	Lin et al. (2013)

[a]Dendritic distribution in the specific EB ring is indicated: C, center ring; A, anterior ring; O, outer ring; P, posterior ring.
[b]Axon distribution in the specific bulb (BU) groups is indicated: i, inferior groups; s, superior groups; a, anterior groups.

projection neuron with small-field dendritic arbors in the medulla and large-field axon terminals in the posterior slope, a brain region analogous to the VMP in the fly (Namiki & Kanzaki, 2018). The axon of MV neurons terminates in both the ipsilateral and the contralateral VMPs, where the VLT neurons further relay visual information to the BU and the L-AOTU bilaterally, suggesting another circuit mechanism of bilateral integration of UV information from both eyes in the fruit fly. Whether the M_6 → VMP → EB pathway mediates head orientation as in the silk moth remains to be addressed.

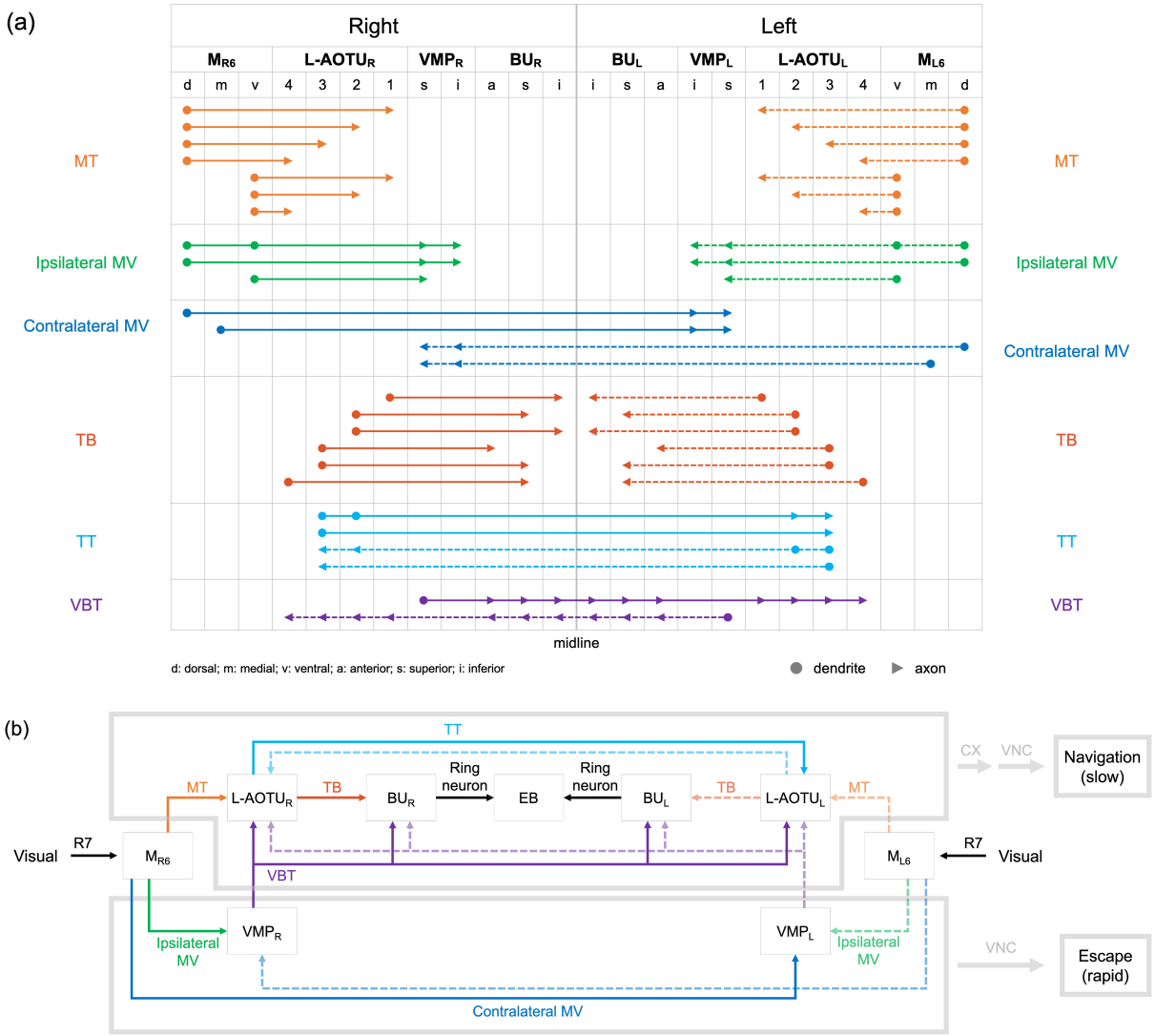

FIGURE 11 Summary of anatomical observations in UV pathways of the *Drosophila* brain. (a) Schematic overview displaying the projection organization in 12 families of visual projection neurons (VPNs). VPNs colored by family (MT neuron = yellow line, ipsilateral MV neuron = green line, contralateral MV = blue, TB neuron = red line, TT neuron = cyan line, and VBT neuron = purple line). VPNs on the right-hand and the left-hand side of the brain are shown in solid line and dotted line, respectively. Filled circles (dendritic) and arrowheads (axonal) point to the target regions of 42 subfamilies. (b) Wiring diagram of the UV circuitry. Arrows indicate the directions of visual information flow. Gray arrows indicate the directions of the purposed visual information flow. The purposed functional implications of the UV circuitry in the brain is shown in gray. M_6, medulla layer 6; L-AOTU, lateral anterior optic tubercle; VMP, ventral medial protocerebrum; BU, bulb; CX, central complex; VNC, ventral nerve cord; d, dorsal; m, medial; v, ventral; a, anterior; s, superior; i, inferior [Color figure can be viewed at wileyonlinelibrary.com]

4.4 | Heading representation

A population of EB output neurons (E-PG) that is responsive to changes in head direction acts as an internal compass for navigation (Seelig & Jayaraman, 2015). The EB consists of five major types of intrinsic ring neurons (R1–R4 and P, Table 7). The R1–R4 neurons are downstream from TB neurons that connect at specific BU microglomeruli to the EB, while the P neurons connect the inferior dorsofrontal protocerebrum (IDFP) to the EB (Hanesch et al., 1989; Renn et al., 1999; Daniels et al., 2008; Lin et al., 2013; Zhang et al., 2013; Martín-Peña et al., 2014). It remains unclear how EB ring neurons orchestrate the compass activity of EB output neurons. Here, we demonstrated parallel visual pathways and stereotyped connectivity from the M_6 columns to the BU glomeruli, indicating a complex computation of bilateral UV information at the EB ring. To generate stable heading representation, GABAergic inhibition by the ring neurons on the E-PG neurons is necessary (Fisher et al., 2019; Kim et al., 2019). However, while GABAergic R2 and R4m neurons convey information to the A ring and the O ring, respectively (Table 7), E-PG neurons have dendrites only in the C ring and the P ring (Lin et al., 2013; Su et al., 2017). As every BU microglomerulus receives UV information, we speculated that heading representation is modulated by interactions among different EB ring neurons.

Parallel and bilateral visual pathways indicated that every EB ring receives visual inputs from bilateral BU glomeruli via ipsilateral

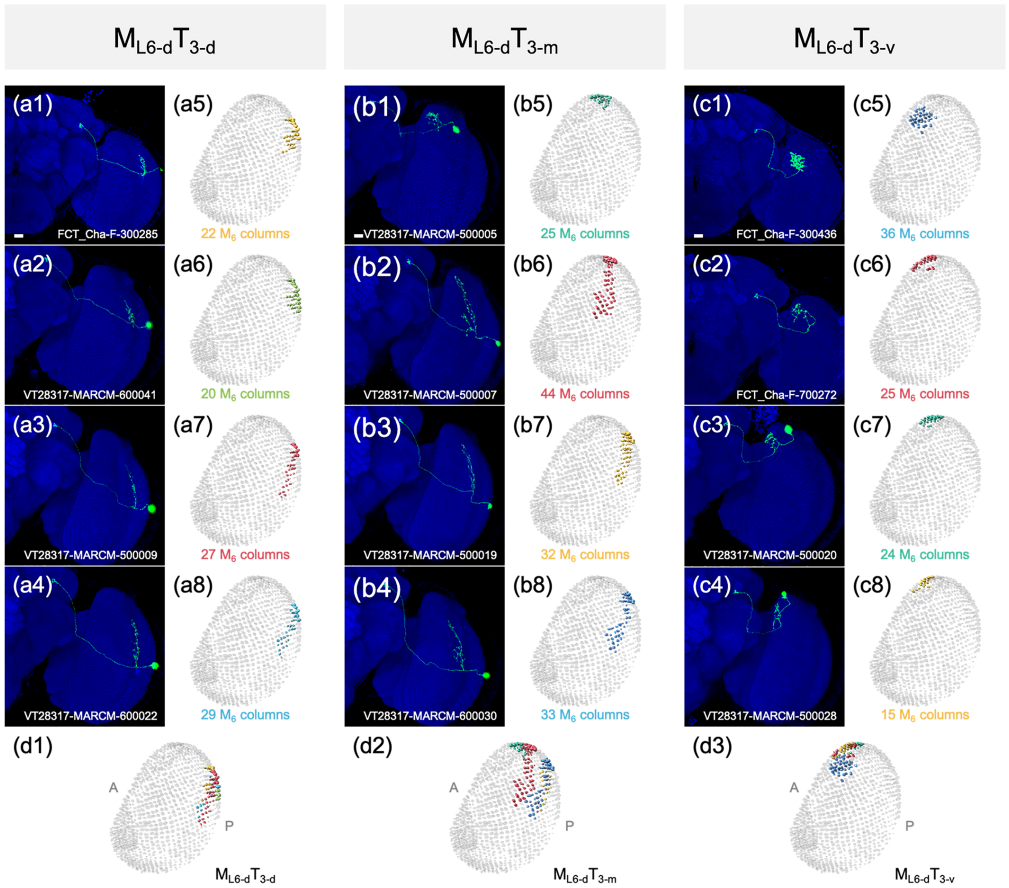

FIGURE 12 Retinotopic map of the $M_{L\text{-}d}T_{L3}$ subfamily. (a) Four representative MT neurons of the $M_{L6\text{-}d}T_{3\text{-}d}$ type. Brain structures immunostained with anti-DLG antibodies (blue). (b) Four representative MT neurons of the $M_{L6\text{-}d}T_{3\text{-}m}$ type. Brain structures immunostained with anti-DLG antibodies (blue). (c) Four representative MT neurons of the $M_{L6\text{-}d}T_{3\text{-}v}$ type. Brain structures immunostained with anti-DLG antibodies (blue). (a5–a8) Skeletal model showing the coverage of medulla layer 6 (M_6) columns by individual $M_{L6\text{-}d}T_{3\text{-}d}$ types in a1–a4. (b5–b8) Skeletal model showing the coverage of M_6 columns by individual $M_{L6\text{-}d}T_{3\text{-}m}$ types in b1–b4. (c5–c8) Skeletal model showing the coverage of M_6 columns by individual $M_{L6\text{-}d}T_{3\text{-}v}$ types in c1–c4. (d) Merged skeletal model of the four $M_{L6\text{-}d}T_{3\text{-}d}$ (d1), four $M_{L6\text{-}d}T_{3\text{-}m}$ (d2), and four $M_{L6\text{-}d}T_{3\text{-}v}$ (d3). Images are frontal views of confocal projections of several adjacent optical sections unless otherwise specified. Scale bars: 20 μm [Color figure can be viewed at wileyonlinelibrary.com]

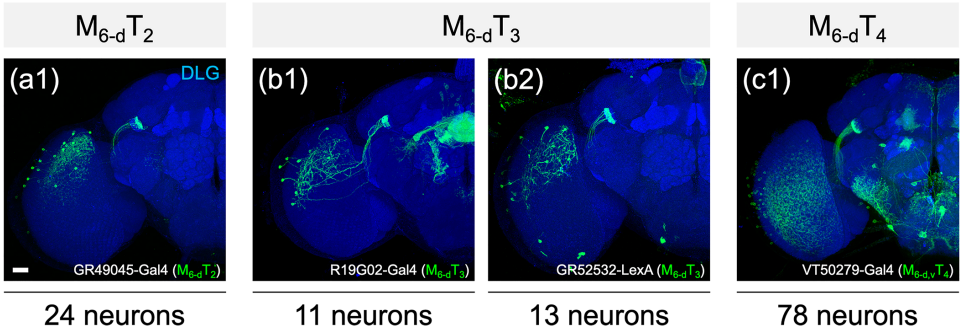

FIGURE 13 Number of column-specific Gal4 and LexA drivers in three MT neurons in each brain hemisphere. Top: Neuron name of column-specific MT neuron. Middle: Expression of column-specific Gal4 and LexA drivers that were visualized with mCD8::GFP. Brain structures immunostained with anti-DLG antibodies (blue). Bottom: Number of neurons for each column-specific MT neuron by counting labeled cells in Gal4 and LexA drivers. Images are mostly frontal views of confocal projections of several adjacent optical sections unless otherwise specified. scale bars: 20 μm [Color figure can be viewed at wileyonlinelibrary.com]

pathways (MT–TB and MV–VBT) and contralateral pathways (MT–TT–TB and MV–VBT), suggesting different heading representations between the two BUs on each side of the EB ring. When a fly encounters a visual cue in the front, only the posterior M_6 receives visual information from the R7 neurons in both eyes (Fischbach & Dittrich, 1989). From here, only dorsal glomeruli of the four L-AOTU columns receive visual input from the posterior M_6 in both brain hemispheres, indicating that some, but not all, BU microglomeruli receive visual inputs. As the visual cue moves to the right, both the posterior and the anterior M_6 in the right brain hemisphere receive visual inputs. From here, all glomeruli in the four L-AOTU columns in the right brain hemisphere receive visual inputs, indicating that all the microglomeruli of the right BU receive visual inputs from both the posterior and the anterior M_6 in the right eye. The difference between the two M_6 visual fields is further represented to the bilateral BUs by commissural TT neurons and ascending VBT neurons, suggesting a circuit mechanism for the heading representation during navigation.

Altogether, the morphological diversity of the visual projection neurons of the M_6 downstream circuitry suggested multi-dimensional processing of UV information via hierarchical, multiple-layer, parallel, and bilateral circuits in the *Drosophila* brain. Notably, the downstream circuitry, which comprises the specialized polarization-sensitive R7 neurons in the dorsal rim area (DRA) of the *Drosophila*'s eye terminate in the medulla dorsal rim area (MEDRA), may differ from the one described herein. Furthermore, the UV-sensitive R7 and the blue-green-sensitive R8 neurons mutually inhibit each other (Schnaitmann et al., 2018). The M_6 downstream circuitry may also be involved in color vision (with an antagonistic action) for green light, as has been shown for TT neurons in locusts (Kinoshita et al., 2007; Pfeiffer & Homberg, 2007). The UV-sensitive R7 neurons also relay visual signals to the lobula via R7–Dm8–Tm5c for UV preference behavior (Gao et al., 2008; Karuppudurai et al., 2014), suggesting that the differentially processed downstream circuits of R7 neurons may convey diverse information to the central brain for color comparison in *Drosophila*. However, the mechanism underlying the circuit interactions between these parallel pathways (R7–Dm8–Tm5c, R7–MT–TB, and R7–MV–VBT) remains to be elucidated. Altogether, this comprehensive visual circuit map provides the basis for studying how the brain uses UV information to guide navigation behavior in *Drosophila*.

ACKNOWLEDGMENTS

We thank Drs. Tzu-Yang Lin and Chi-Hon Lee for their critical comments to improve the manuscript. We thank the Vienna *Drosophila* Resource Center and Bloomington Stock Center for the fly stocks. We are grateful to the *FlyCircuit* database from the NCHC (National Center for High-Performance Computing) and NTHU (National Tsing Hua University) for providing original single-neuron images.

PEER REVIEW

The peer review history for this article is available at https://publons.com/publon/10.1002/cne.25068.

CONFLICT OF INTEREST

The authors declare no competing interests.

AUTHOR CONTRIBUTIONS

Chu-Yi Tai, An-Lun Chin, and Ann-Shyn Chiang planned the study and analyzed the data. Chu-Yi Tai performed imaging experiments, *FlyCircuit* data analysis. Chu-Yi Tai and Ann-Shyn Chiang wrote the paper. Ann-Shyn Chiang supervised the project. All authors had access to all the data in this study and take responsibility for the integrity of the data and the accuracy of the data analysis.

DATA AVAILABILITY STATEMENT

The data that support the findings of this study are available from the corresponding author upon request.

ORCID

Ann-Shyn Chiang https://orcid.org/0000-0001-9668-7115

REFERENCES

Amin, H., & Lin, A. C. (2019). Neuronal mechanisms underlying innate and learned olfactory processing in *Drosophila*. *Current Opinion in Insect Science*, *36*, 9–17. https://doi.org/10.1016/j.cois.2019.06.003.

Behnia, R., & Desplan, C. (2015). Visual circuits in flies: Beginning to see the whole picture. *Current Opinion in Neurobiology*, *34*, 125–132. https://doi.org/10.1016/j.conb.2015.03.010.

Chiang, A. S., Lin, C. Y., Chuang, C. C., Chang, H. M., Hsieh, C. H., Yeh, C. W., Shih, C. T., Wu, J. J., Wang, G. T., Chen, Y. C., Wu, C. C., Chen, G. Y., Ching, Y. T., Lee, P. C., Lin, C. Y., Lin, H. H., Wu, C. C., Hsu, H. W., Huang, Y. A., … Hwang, J. K. (2011). Three-dimensional reconstruction of brain-wide wiring networks in *Drosophila* at single-cell resolution. *Current Biology*, *21*, 1–11. https://doi.org/10.1016/j.cub.2010.11.056.

Chin, A. L., Lin, C. Y., Fu, T. F., Dickson, B. J., & Chiang, A. S. (2014). Diversity and wiring variability of visual local neurons in the *Drosophila* medulla M6 stratum. *Journal of Comparative Neurology*, *522*, 3795–3816. https://doi.org/10.1002/cne.23622.

Daniels, R. W., Gelfand, M. V., Collins, C. A., & DiAntonio, A. (2008). Visualizing glutamatergic cell bodies and synapses in *Drosophila* larval and adult CNS. *Journal of Comparative Neurology*, *508*, 131–152. https://doi.org/10.1002/cne.21670.

el Jundi, B., Pfeiffer, K., Heinze, S., & Homberg, U. (2014). Integration of polarization and chromatic cues in the insect sky compass. *Journal of Comparative Physiology A*, *200*, 575–589. https://doi.org/10.1007/s00359-014-0890-6.

Feinberg, E. H., VanHoven, M. K., Bendesky, A., Wang, G., Fetter, R. D., Shen, K., & Bargmann, C. I. (2008). GFP reconstitution across synaptic partners (GRASP) defines cell contacts and synapses in living nervous systems. *Neuron*, *57*, 353–363. https://doi.org/10.1016/j.neuron.2007.11.030.

Fischbach, K. F., & Dittrich, A. P. M. (1989). The optic lobe of *Drosophila melanogaster*. I. a Golgi analysis of wild-type structure. *Cell and Tissue Research*, *258*, 441–475. https://doi.org/10.1007/BF00218858.

Fisher, Y. E., Lu, J., D'Alessandro, I., & Wilson, R. I. (2019). Sensorimotor experience remaps visual input to a heading-direction network. *Nature*, *576*, 121–125. https://doi.org/10.1038/s41586-019-1772-4.

Gao, S., Takemura, S., Ting, C. Y., Huang, S., Lu, Z., Luan, H., Rister, J., Thum, A. S., Yang, M., Hong, S. T., Wang, J. W., Odenwald, W. F., White, B. H., Meinertzhagen, I. A., & Lee, C. H. (2008). The neural substrate of spectral preference in *Drosophila*. *Neuron*, *60*, 328–342. https://doi.org/10.1016/j.neuron.2008.08.010.

Guo, F., Holla, M., Díaz, M. M., & Rosbash, M. (2018). A circadian output circuit controls sleep-wake arousal in *Drosophila*. *Neuron*, *100*, 624–635. https://doi.org/10.1016/j.neuron.2018.09.002

Hanesch, U., Fischbach, K. F., & Heisenberg, M. (1989). Neuronal architecture of the central complex in *Drosophila melanogaster*. *Cell and Tissue Research*, *257*, 343–366. https://doi.org/10.1007/BF00261838.

Heinze, S., Florman, J., Asokaraj, S., el Jundi, B., & Reppert, S. M. (2013). Anatomical basis of sun compass navigation II: The neuronal composition of the central complex of the monarch butterfly. *Journal of Comparative Neurology*, *521*, 267–298. https://doi.org/10.1002/cne.23214.

Homberg, U., Hofer, S., Pfeiffer, K., & Gebhardt, S. (2003). Organization and neural connections of the anterior optic tubercle in the brain of the locust, *Schistocerca gregaria*. *Journal of Comparative Neurology*, *462*, 415–430. https://doi.org/10.1002/cne.10771.

Karuppudurai, T., Lin, T. Y., Ting, C. Y., Pursley, R., Melnattur, K. V., Diao, F., White, B. H., Macpherson, L. J., Gallio, M., Pohida, T., & Lee, C. H. (2014). A hard-wired glutamatergic circuit pools and relays UV signals to mediate spectral preference in *Drosophila*. *Neuron*, *81*, 603–615. https://doi.org/10.1016/j.neuron.2013.12.010.

Kim, S. S., Hermundstad, A. M., Romani, S., Abbott, L. F., & Jayaraman, V. (2019). Generation of stable heading representations in diverse visual scenes. *Nature*, *576*, 126–131. https://doi.org/10.1038/s41586-019-1767-1.

Kinoshita, M., Pfeiffer, K., & Homberg, U. (2007). Spectral properties of identified polarized-light sensitive interneurons in the brain of the desert locust *Schistocerca gregaria*. *Journal of Experimental Biology*, *210*, 1350–1361. https://doi.org/10.1242/jeb.02744.

Lamaze, A., Krätschmer, P., Chen, K. F., Lowe, S., & Jepson, J. E. (2018). A wake-promoting circadian output circuit in *Drosophila*. *Current Biology*, *28*, 3098–3105. https://doi.org/10.1016/j.cub.2018.07.024

Lee, T., & Luo, L. (1999). Mosaic analysis with a repressible cell marker for studies of gene function in neuronal morphogenesis. *Neuron*, *22*, 451–461. https://doi.org/10.1016/S0896-6273(00)80701-1.

Lin, C. Y., Chuang, C. C., Hua, T. E., Chen, C. C., Dickson, B. J., Greenspan, R. J., & Chiang, A. S. (2013). A comprehensive wiring diagram of the protocerebral bridge for visual information processing in the *Drosophila* brain. *Cell Reports*, *3*, 1739–1753. https://doi.org/10.1016/j.celrep.2013.04.022.

Martín-Peña, A., Acebes, A., Rodríguez, J. R., Chevalier, V., Casas-Tinto, S., Triphan, T., Strauss, R., & Ferrús, A. (2014). Cell types and coincident synapses in the ellipsoid body of *Drosophila*. *European Journal of Neuroscience*, *39*, 1586–1601. https://doi.org/10.1111/ejn.12537.

Namiki, S., Dickinson, M. H., Wong, A. M., Korff, W., & Card, G. M. (2018). The functional organization of descending sensory-motor pathways in *Drosophila*. *eLife*, *7*, e34272. https://doi.org/10.7554/eLife.34272.

Namiki, S., & Kanzaki, R. (2018). Morphology of visual projection neurons supplying premotor area in the brain of the silkmoth *Bombyx mori*. *Cell and Tissue Research*, *374*, 497–515. https://doi.org/10.1007/s00441-018-2892-0.

Omoto, J. J., Keleş, M. F., Nguyen, B. C. M., Bolanos, C., Lovick, J. K., Frye, M. A., & Hartenstein, V. (2017). Visual input to the *Drosophila* central complex by developmentally and functionally distinct neuronal populations. *Current Biology*, *27*, 1098–1110. https://doi.org/10.1016/j.cub.2017.02.063.

Otsuna, H., Shinomiya, K., & Ito, K. (2014). Parallel neural pathways in higher visual centers of the *Drosophila* brain that mediate wavelength-specific behavior. *Frontiers in Neural Circuits*, *8*, 8. https://doi.org/10.3389/fncir.2014.00008.

Pfeiffer, K., & Homberg, U. (2007). Coding of azimuthal directions via time-compensated combination of celestial compass cues. *Current Biology*, *17*, 960–965. https://doi.org/10.1016/j.cub.2007.04.059.

Pfeiffer, K., & Kinoshita, M. (2012). Segregation of visual inputs from different regions of the compound eye in two parallel pathways through the anterior optic tubercle of the bumblebee (*Bombus ignitus*). *Journal of Comparative Neurology*, *520*, 212–229. https://doi.org/10.1002/cne.22776.

Renn, S. C. P., Armstrong, J. D., Yang, M., Wang, Z., An, X., Kaiser, K., & Taghert, P. H. (1999). Genetic analysis of the *Drosophila* ellipsoid body neuropil: Organization and development of the central complex. *Journal of Neurobiology*, *41*, 189–207. https://doi.org/10.1002/(SICI)1097-4695(19991105)41:2<189::AID-NEU3>3.0.CO;2-Q.

Sanes, J. R., & Zipursky, S. L. (2010). Design principles of insect and vertebrate visual systems. *Neuron*, *66*, 15–36. https://doi.org/10.1016/j.neuron.2010.01.018.

Schnaitmann, C., Haikala, V., Abraham, E., Oberhauser, V., Thestrup, T., Griesbeck, O., & Reiff, D. F. (2018). Color processing in the early visual system of *Drosophila*. *Cell*, *172*, 318–330. https://doi.org/10.1016/j.cell.2017.12.018.

Seelig, J. D., & Jayaraman, V. (2013). Feature detection and orientation tuning in the *Drosophila* central complex. *Nature*, *503*, 262–266. https://doi.org/10.1038/nature12601.

Seelig, J. D., & Jayaraman, V. (2015). Neural dynamics for landmark orientation and angular path integration. *Nature*, *521*, 186–191. https://doi.org/10.1038/nature14446.

Shih, C. T., Sporns, O., Yuan, S. L., Su, T. S., Lin, Y. J., Chuang, C. C., Wang, T. Y., Lo, C. C., Greenspan, R. J., & Chiang, A. S. (2015). Connectomics-based analysis of information flow in the *Drosophila* brain. *Current Biology*, *25*, 1249–1258. https://doi.org/10.1016/j.cub.2015.03.021.

Song, B. M., & Lee, C. H. (2018). Toward a mechanistic understanding of color vision in insects. *Frontiers in Neural Circuits*, *12*, 16. https://doi.org/10.3389/fncir.2018.00016.

Su, T. S., Lee, W. J., Huang, Y. C., Wang, C. T., & Lo, C. C. (2017). Coupled symmetric and asymmetric circuits underlying spatial orientation in fruit flies. *Nature Communications*, *8*, 1–15. https://doi.org/10.1038/s41467-017-00191-6.

Takemura, S., Bharioke, A., Lu, Z., Nern, A., Vitaladevuni, S., Rivlin, P. K., Katz, W. T., Olbris, D. J., Plaza, S. M., Winston, P., Zhao, T., Horne, J. A., Fetter, R. D., Takemura, S., Blazek, K., Chang, L. A., Ogundeyi, O., Saunders, M. A., Shapiro, V., … Chklovskii, D. B. (2013). A visual motion detection circuit suggested by *Drosophila* connectomics. *Nature*, *500*, 175–181. https://doi.org/10.1038/nature12450.

Timaeus, L., Geid, L., Sancer, G., Wernet, M. F., & Hummel, T. (2020). Parallel visual pathways with topographic versus non-topographic organization connect the *Drosophila* eyes to the central brain. *bioRxiv*, 2020.04.11.037333. https://doi.org/10.1101/2020.04.11.037333

Warren, T. L., Giraldo, Y. M., & Dickinson, M. H. (2019). Celestial navigation in *Drosophila*. *Journal of Experimental Biology*, *222*. https://doi.org/10.1242/jeb.186148.

Zeller, M., Held, M., Bender, J., Berz, A., Heinloth, T., Hellfritz, T., & Pfeiffer, K. (2015). Transmedulla neurons in the sky compass network of the honeybee (*Apis mellifera*) are a possible site of circadian input. *PLoS One*, *10*, e0143244. https://doi.org/10.1371/journal.pone.0143244.

Zhang, Z., Li, X., Guo, J., Li, Y., & Guo, A. (2013). Two clusters of GABAergic ellipsoid body neurons modulate olfactory labile memory in *Drosophila*. *Journal of Neuroscience*, *33*, 5175–5181. https://doi.org/10.1523/JNEUROSCI.5365-12.2013.

Zheng, Z., Lauritzen, J. S., Perlman, E., Robinson, C. G., Nichols, M., Milkie, D., Torrens, O., Price, J., Fisher, C. B., Sharifi, N., Calle-Schuler, S. A., Kmecova, L., Ali, I. J., Karsh, B., Trautman, E. T., Bogovic, J. A., Hanslovsky, P., Jefferis, G. S. X. E., Kazhdan, M., … Bock, D. D. (2018). A complete electron microscopy volume of the brain of adult *Drosophila melanogaster*. *Cell*, *174*, 730–743. https://doi.org/10.1016/j.cell.2018.06.019.

How to cite this article: Tai C-Y, Chin A-L, Chiang A-S. Comprehensive map of visual projection neurons for processing ultraviolet information in the *Drosophila* brain. *J Comp Neurol*. 2021;529:1988–2013. https://doi.org/10.1002/cne.25068